Surveys in Geophysics
https://doi.org/10.1007/s10712-026-09928-9

Unresolved Questions in Subauroral Science: Exploring Key Challenges in Physics and Chemistry

Bea Gallardo-Lacourt[1,2] · Maxime Grandin[3] · Aurélie Marchaudon[4] · Mathieu Barthelemy[5,6]

Received: 2 May 2025 / Accepted: 2 January 2026

Abstract
The subauroral region, located equatorward of the auroral oval, is a highly dynamic and complex interface between the magnetosphere, ionosphere, and thermosphere. While traditionally associated with stable optical structures such as stable auroral red arcs, recent observations have revealed a wide range of transient and extreme phenomena—such as subauroral ion drifts and strong thermal emission velocity enhancement—which highlight the region's variability and intense coupling. The dynamics of the subauroral ionosphere are not only influenced by processes occurring at higher latitudes within the auroral oval but are also shaped by interactions across multiple regions of geospace, including the inner magnetosphere, ring current, inner plasma sheet, and the lower-altitude thermosphere. This growing body of research has underscored both the scientific richness of the subauroral region and the many outstanding questions regarding its drivers and chemical processes. In this paper, we present a in-depth review of observed subauroral structures, available ground-based and satellite datasets, and current modeling efforts aimed at understanding the region's dynamics. We also examine the state of knowledge surrounding the subauroral ionospheric/thermospheric chemistry and outline critical gaps that require further investigation. Finally, we discuss the pressing need for targeted experiments and new space missions to advance our understanding of this key geospace region.

Keywords Subauroral · Dynamics · Physics · Chemistry

1 Introduction

The subauroral ionosphere, as the name suggests, is a region located immediately equatorward of the auroral oval. From the perspective of the magnetosphere and magnetic field topology, this is an area highly influenced by the nightside transition region where Earth's magnetic field transitions from the highly stretched, closed magnetic field lines of the plasma sheet in the magnetotail to the more dipole-like closed field lines of the inner magnetosphere. The nightside transition region, generally found at radial distances within 6–12 R_E (Gabrielse et al. 2023), acts as a critical interface between the inner plasma sheet and the inner magnetosphere, where interactions with the ring current drive dynamic

Extended author information available on the last page of the article

processes such as flow braking, dipolarization, and particle injections. These magnetospheric disturbances are mapped along magnetic field lines to the subauroral ionosphere, where they manifest as subauroral polarization streams (SAPS), enhanced ion drifts, and localized ionospheric heating–making the subauroral region a key ionospheric counterpart to the dynamics of the transition region.

One of the defining features of the subauroral region is the presence of westward plasma flows, particularly in the pre-midnight sector. These westward flows or ion drift velocities are commonly referred to as subauroral polarization streams (SAPS) (Foster and Burke 2002), a term that encompasses both wide (~ 5°) and moderate (~500 m/s) flows, as well as very narrow (< 1°) and fast (>1 km/s) flows. However, a distinction is often made in the literature where SAPS is frequently used to describe the moderate flows, while the older term of subauroral ion drift (SAID), also known as polarization jets, is reserved for the faster flows. For clarity and simplicity, this paper adopts the latter convention.

The generation mechanisms behind these westward flows have been a subject of extensive research and debate, with two primary theories emerging. One proposed mechanism is the current generator theory, which explains that, in the pre-midnight sector, the Region 1 and Region 2 field-aligned currents flow out of the ionosphere at higher latitudes and into it at lower latitudes. To maintain current continuity, a poleward-directed Pedersen current closes the system within the ionosphere. This current is accompanied by a poleward-directed electric field. In the northern (southern) hemisphere, where the magnetic field points toward (away from) Earth, the $\mathbf{E} \times \mathbf{B}$ drift—which arises from the Lorentz force in a collisionless plasma—results in a westward plasma velocity, corresponding to SAPS or SAID. This mechanism was first introduced by Anderson et al. (1991) and has been extensively discussed in later studies (e.g., Anderson et al. 1993, 2001).

The second prominent theory, known as the voltage generator mechanism, arises from the single particle motion. In the pre-midnight sector, the inner boundary of hot plasma sheet ions penetrates further Earthward than that of electrons, creating a tailward-polarizing electric field consistent with the observed westward flows in the subauroral region. Originally proposed by Southwood and Wolf (1978), this mechanism has been refined and debated in subsequent literature (e.g., Mishin 2013; Mishin et al. 2017; Mishin 2023).

While the generation mechanism of subauroral flows remains under active debate, it is possible that both processes contribute, or that the dominant mechanism varies from event to event. Localized in situ measurements from upcoming missions should help clarify this issue.

These westward flows, and the associated poleward electric fields, play a critical role in particle energization and contribute to the intricate dynamics of the subauroral region. They are closely tied to the variety of optical phenomena observed in this region. Figure 1 shows an example of SAPS/SAID provided by Foster and Burke (2002). The first two panels (Fig. 1a) represent the ion velocity (positive values indicate westward flow) and the electron density measured by the Millstone Hill incoherent scatter radar. The three lower panels (Fig. 1b) display conjugate observations of the electron and ion precipitating fluxes, along with horizontal drifts (positive values indicate westward motion) by the DMSP-13 satellite at ~850 km altitude. The figure highlights the broader SAPS flows located equatorward of the auroral oval, with the electron equatorward boundary marked by a solid black line. The radar measurements clearly reveal a narrow flow exceeding 1.5 km/s channel embedded within the SAPS, known as the SAID.

In this paper, we examine the various phenomena occurring in the subauroral regions, their importance, and the current methods used to measure and model them. We highlight the limitations of existing approaches in effectively capturing subauroral dynamics through

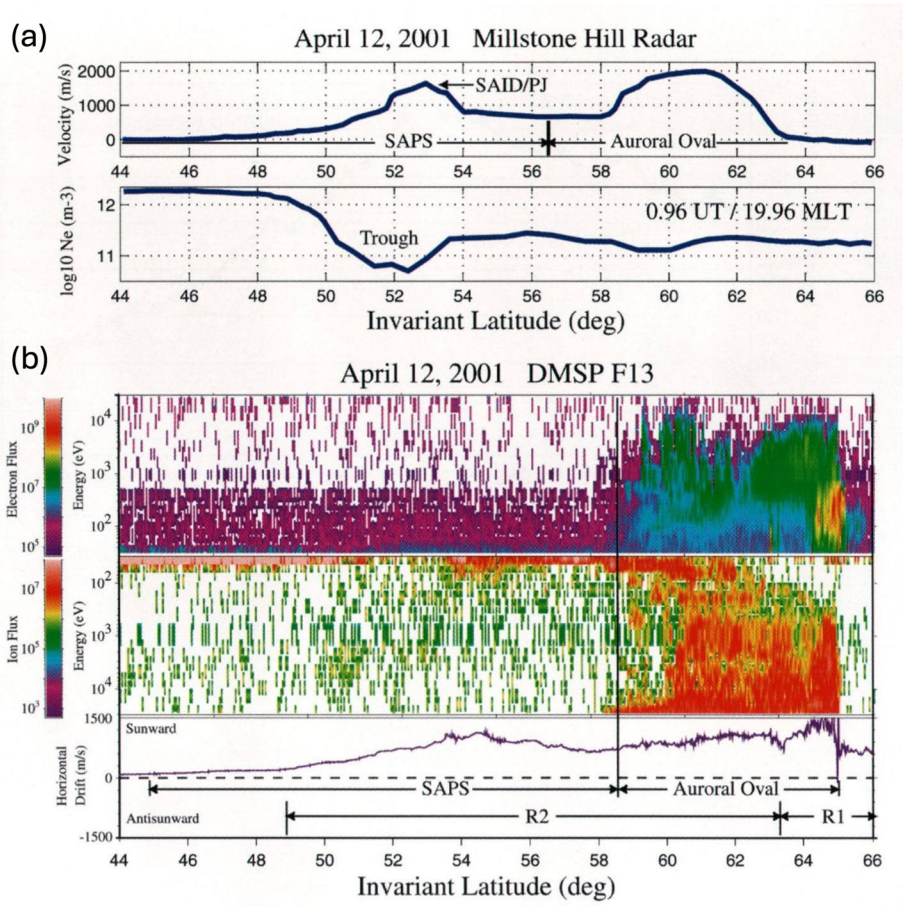

Fig. 1 Simultaneous SAPS measurements using two instruments: **a** The Millstone Hill Incoherent Scatter Radar. The upper panel displays westward drifts (positive values), while the lower panel shows electron density, with the trough region highlighted by lower density values. The signature of a SAID/polarization jet (PJ) within the SAPS structure is indicated. **b** Conjugate DMSP F13 satellite measurements. The first two panels show precipitating fluxes of electrons and ions, enabling determination of the auroral oval's equatorward boundary. The final panel presents plasma drift measurements from DMSP, which align with the radar observations (from Foster and Burke 2002)

both observational data and modeling efforts. Additionally, we explore ongoing efforts to analyze atmospheric chemistry at these altitudes and the significant challenges this presents. Furthermore, we discuss notable community initiatives and missions that focus on the subauroral region, contributing substantially to advancing scientific understanding of its dynamics. Finally, we outline key open questions and propose potential directions for future research in subauroral science.

2 Observed Phenomena in the Subauroral Region

Some of the phenomena that occur in the subauroral ionosphere include Stable Auroral Red (SAR) arcs, STEVE (Strong Thermal Emission Velocity Enhancement), and dune aurora, among others. In this section, we will discuss some of these phenomena, illustrated with examples given in Fig. 2.

Stable Auroral Red (SAR; Fig. 2a, b) arcs are an optical manifestation of magnetosphere–ionosphere coupling, typically associated with the plasma trough, a subauroral region characterized by depleted plasma density. While traditionally observed during storm-time conditions and noted for their spectral purity in the 630.0 nm emission band (e.g., Kozyra et al. 1997), recent observations have detected green emissions linked to SAR arcs (Mendillo et al. 2016), challenging the notion of SAR arcs as stable optical structures. These studies have also revealed that SAR arcs, while spanning a relatively narrow latitudinal region (~5 degrees), can extend widely in longitude (several hours in MLT).

Statistical analyses of SAR arcs highlight their relationships with solar and geomagnetic activity, as well as seasonal and hemispheric variations. Lobzin and Pavlov (1999) demonstrated that SAR arc electron temperatures are primarily influenced by additional heating from ring current ion interactions, with temperature variations reflecting changes in ring current parameters on timescales of minutes to hours. The peak emission rate typically occurs between 300 and 500 km altitude, depending on the vertical distribution of the neutral species involved in quenching processes, as well as the altitude-dependent production

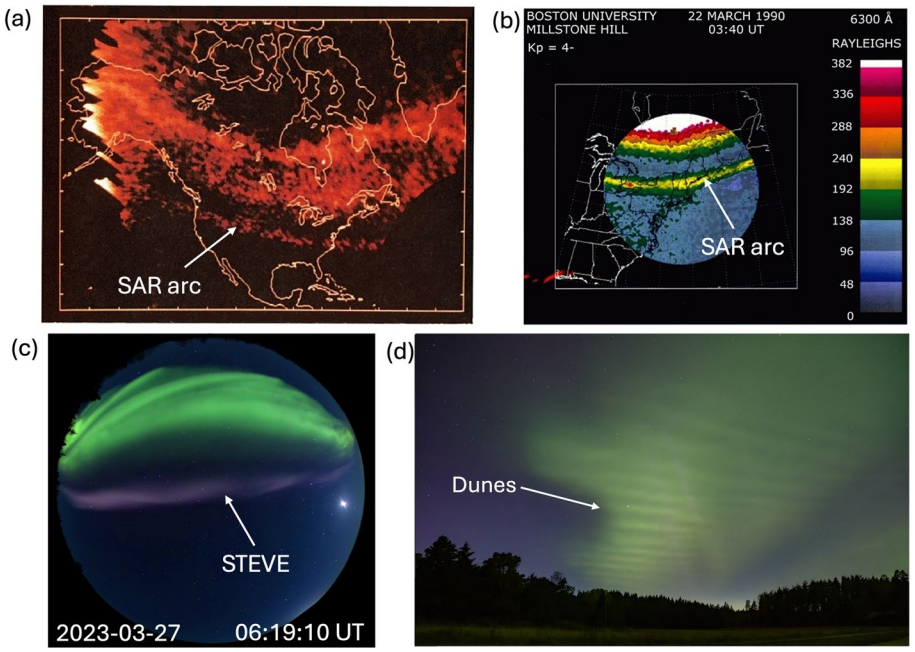

Fig. 2 Examples of various optical phenomena observed in the subauroral region: **a**, **b** SAR arc observations (adapted from Craven et al. 1982 and Mendillo et al. 2013), **c** STEVE observation courtesy of Jeremy Kuzub and the AurorEye Project (https://doi.org/https://auroreye.ca/, figure adapted from Gallardo-Lacourt et al. 2024), and **d** Dunes observation example courtesy of Pirjo Koski

of excited oxygen atoms (Kozyra et al. 1997, and references therein). Takagi et al. (2018) found that SAR arcs often form pre-midnight during the recovery phase of substorms, with seasonal studies (e.g., Fok et al. 1993; Kozyra et al. 1997) indicating weaker emissions during summer months. Recent simultaneous observations in both hemispheres have further enhanced our understanding of SAR arc dynamics. During an event taking place on 1 June 2013, Martinis et al. (2019) found differences in morphology and brightness of two conjugate SAR arcs that otherwise exhibited a similar spatial extent and equatorward motion, highlighting that SAR arcs are the manifestation of a complex coupling between the inner magnetosphere acting as the energy source and the local conditions at the ionospheric foot point of the concerned geomagnetic field lines. In a study of the 17 March 2015 St Patrick storm, Hong et al. (2020) revealed that interhemispheric asymmetries of SAR arcs can also include differences in latitudinal extent and even time of formation of the northern-vs-southern SAR arc, hinting at a possible role of the ionospheric trough, which exhibits seasonal variations.

A subcategory of SAR arcs, termed detached SAR arcs (Shiokawa et al. 2009), has been reported during non-storm-time substorms. These arcs are separated from the main oval and are thought to be linked to ring current particle injections in the inner magnetosphere. While they share many characteristics with classical SAR arcs, they differ in latitudinal width, temporal evolution, and storm association, suggesting distinct generation mechanisms (e.g., Takagi et al. 2018; Gololobov et al. 2023).

Statistical analyses show that strong horizontal flows are present in only 22% of events, with no clear effect on emission intensity, indicating that flow is not a necessary condition. Detached SAR arcs correlate more strongly with the geomagnetic Ap, AE, and PCN indices than with F10.7 or SYM-H, pointing to stronger links with substorm activity than with ring current strength or solar flux. Emission intensities at 630.0 nm scale with electron temperature, supporting electron heating as the primary driver (Inaba et al. 2020, 2021). The increase in electron temperature following detachment further suggests enhanced downward heat flux (Gololobov et al. 2023).

The energy mechanisms driving SAR arcs remain under active investigation. Proposed sources include heat conduction and soft electron precipitation from the inner magnetosphere to the ionosphere, driven by interactions between energetic ring current ions and plasmaspheric electrons (Rees and Roble 1975; Fok et al. 1991, 1993). This energy transfer is influenced by plasmaspheric conditions and the composition and energy of ring current ions, with different ion species (O^+, H^+, He^+) dominating during specific storm phases. Recent data combining Van Allen Probes, measuring plasma parameters and waves in the radiation belts (apogee at $\sim 6R_E$), with ground-based observations show low-energy ion fluxes near magnetic field lines linked to SAR arcs, though direct evidence of key wave–particle interactions such as EMIC waves or Landau damping remains limited (e.g., Lanzerotti et al. 1978; Anderson et al. 1992; Wang et al. 2019). Additional mechanisms, including the role of large electric fields like SAPS and SAID structures, plasma waves, and ion–neutral frictional heating, suggest that SAR arcs could be produced by a combination of processes (e.g., Jordanova et al. 1999; Sazykin et al. 2002). These complexities underscore the need for further quantitative investigations to unravel the interplay of factors contributing to SAR arc formation and evolution.

In recent years, a new phenomenon has been detected in the subauroral ionosphere, marking the first time an optical phenomenon has been directly tied to subauroral ion drifts. Known as STEVE (Strong Thermal Emission Velocity Enhancement; Fig. 2c), this optical feature was initially discovered by citizen scientists and is consistently observed alongside extreme subauroral ion drifts (MacDonald et al. 2018; Archer et al. 2019a). Figure 2c was

captured by the AurorEye project (https://doi.org/https://auroreye.ca/), a system developed, deployed, and operated by citizen scientists. STEVE appears in the night sky as a narrow purple or mauve arc that propagates westward within the subauroral ionosphere (Gallardo-Lacourt et al. 2018; Nishimura et al. 2019). It is sometimes accompanied by a distinct green, ray-like structure referred to as the "picket fence", and some very small-scale (<1 km across) green emissions, dubbed "streaks", have also been reported during STEVE events (Semeter et al. 2020). STEVE itself exhibits a unique optical spectrum that sets it apart from typical auroral emissions. While auroras display an emission spectrum consisting of discrete lines and bands, STEVE's spectrum is continuous (Gillies et al. 2019). In addition, STEVE has been observed under a wide range of geomagnetic conditions, including quiet times (e.g., Gallardo-Lacourt et al. 2024; Nishimura et al. 2024), minor storms (e.g., Gallardo-Lacourt et al. 2018), and major storm events (e.g., Martinis et al. 2022). However, the presence of substorms and particle injections appears to be a ubiquitous magnetospheric feature associated with most STEVE occurrences.

The mechanisms responsible for STEVE's distinctive spectrum, as well as the formation of the picket fence, have been the subject of intense scientific debate (Harding et al. 2020; Mishin and Streltsov 2021; Gasque et al. 2023; Liang and Donovan 2024). These mechanisms have been proposed by considering STEVE's spectral characteristics, spatial location, approximate altitude, and the extreme subauroral ion drifts (SAIDs) associated with it. Martinis et al. (2022) reported SAID velocities of at least 10 km/s during the transition from a SAR arc to STEVE (see also Martinis et al. 2021; Gillies et al. 2023), while more recent studies have estimated values approaching 20 km/s (Zhang et al. 2024). However, in the absence of in situ measurements at the altitudes where STEVE and the picket fence occur–estimated to lie between 100 km and 250 km (e.g., Archer et al. 2019b; Liang et al. 2019)—identifying the exact physical drivers of STEVE and its associated features remains a significant challenge.

In addition to SAR arcs and STEVE, another class of subauroral arcs has been reported in the literature. In the dusk sector, detached arcs were first introduced to describe aurora-like emissions located equatorward of the main auroral oval (Anger et al. 1978). Although they occur in the subauroral region, their optical and spectroscopic characteristics differ from both SAR arcs and STEVE. Anger et al. (1978) noted that detached arcs are most commonly observed in the 391.4 nm and 557.7 nm emission lines, with little to no enhancement in the 630.0 nm line. They also suggested that detached arcs are relatively rare. Early interpretations proposed that these arcs result from plasma sheet particles left behind following the contraction of the auroral oval (Moshupi et al. 1979). More recent studies, however, indicate that detached arcs are associated with localized enhancements of low-energy electrons (0.1–2 keV) near the inner edge of the electron plasma sheet (Yadav et al. 2021). In recent years, detached arcs—and subauroral dynamics more broadly—have received renewed scientific attention.

Another dark-sky optical phenomenon discovered and investigated through citizen science is the dunes (or dune aurora), an auroral form characterized by a horizontal, wave-like pattern embedded within the dim, diffuse green aurora (Palmroth et al. 2020). Although this phenomenon does not typically occur in the subauroral region, its proximity to the equatorward boundary of electron precipitation within the auroral oval makes it highly relevant for understanding the dynamic behavior within and adjacent to the subauroral region. In the limited number of cases reported in the literature, dunes appear as a field of bright, roughly parallel bands located on the equatorward edge of the auroral oval, slowly drifting with respect to a fixed ground observer. Figure 2d shows an example of dunes captured by citizen scientist Pirjo Koski. This observation, taken on October 7, 2015, in Laitila,

Western Finland, is one of the earliest documented recordings of the dunes phenomenon. Triangulation analysis of dunes events have determined that the optical emission is produced at about 100 km altitude (Palmroth et al. 2020). In an event study, Grandin et al. (2021) estimated the drifting velocity to be on the order of 200 m/s, which could result from the combination of the intrinsic (i.e., with respect to the air mass) propagation speed of the structure supporting the dunes and an elevated neutral wind speed. This interpretation assumes that the dunes appear when particle precipitation excites the atmospheric species near the mesopause in presence of an atmospheric wave which modulates the neutral density in the horizontal plane, as was proposed by Palmroth et al. (2020). Satellite-based evidence supporting this hypothesis was provided by Grandin et al. (2021), as the presence of a sharp temperature inversion layer below the mesopause was found during the studied event. Such a structure can sustain suitable conditions for a large-scale atmospheric wave known as the mesospheric bore to propagate near the mesopause (Dewan and Picard 1998, 2001).

While detailed occurrence statistics are not yet available, the few dune events reported in Palmroth et al. (2020) suggested that October might favor their formation. This led Izvekova et al. (2025) to propose that the conditions producing the dunes could involve the formation of a nonlinear periodic duct for acoustic waves resulting from high-speed meteor showers creating a dusty plasma around 100 km altitude, as October corresponds to the time when the Draconid meteor shower occurs. On the other hand, He et al. (2023) investigated a dune event occurring at the same time as sawtooth aurora and rather suggested that the dunes are produced by the periodic modulation of the precipitating particle flux by exohiss waves at the plasmapause. This highlights that the formation mechanism of the dunes is currently not identified, and further research is needed to shed light on this phenomenon, which was for instance observed by citizen scientists during the 10 May 2024 superstorm (Grandin et al. 2024). Although it is still unclear whether it is always the case, the vast majority of dune events reported so far have been observed at the equatorward edge of the auroral oval, potentially suggesting that the dunes may be an auroral form requiring processes typically occurring close to the subauroral latitudes.

Particle precipitation in the subauroral region consists not only of electrons, responsible for the majority of the studied optical emission forms, but also of protons at so-called auroral energies of a few kiloelectronvolts, generally occurring at the equatorward edge of the auroral oval (Galand and Chakrabarti 2006). Most studies of optical emissions associated with precipitating protons have focused on the hydrogen Balmer series, especially Hα at 656.3 nm and Hβ at 486.1 nm, and on the Lyman-α emission line at 121.6 nm (Galand 2001, and references therein). However, little research has investigated optical emissions resulting from the excitation of neutral atmospheric species by secondary electrons in the presence of proton precipitation. While the production of secondary electrons is well known (e.g., Eather 1968; Lummerzheim et al. 2001), a recent study using citizen science data by Nishimura et al. (2022) demonstrated that secondary electrons can lead to the production of green and red emissions at subauroral latitudes. Specifically, in the event analyzed by Nishimura et al. (2022), green diffuse emissions appeared equatorward of the auroral oval and propagated further equatorward. These green diffuse emissions were identified as proton aurora due to the presence of Hβ emissions and ion precipitation. The red arc was associated with the green emissions, indicating the role of secondary electrons. The green emissions decayed more rapidly than the red arc, which was subsequently identified as a SAR arc. This transition, as reported by Nishimura et al. (2022), suggests that the SAR arc was initiated by secondary electrons associated with proton precipitation. Following this observation, citizen scientists introduced then terms such as red and green diffuse

aurora" (RAGDA) and isolated proton aurora" (IPA) to describe these types of structures (Herlingshaw et al. 2024).

For a more comprehensive discussion, see the review on subauroral structures by Gallardo-Lacourt et al. (2021).

3 Revisiting the Available Datasets

In recent years, the renewed interest in subauroral research has prompted a thorough review and revision of existing datasets. Notably, Laakso and Pfaff (2023) revisited plasma drift measurements obtained by the Dynamic Explorer-2 (DE-2) satellite during its 18-month mission (August 1981 to February 1983). DE-2 was a satellite operating on an high-inclination elliptical orbit with a remarkably low perigee at about 300 km altitude. Figure 3 illustrates an example of the intense electric field and rapid plasma drift identified by the authors through the re-analysis of DE-2 data. Their analysis identified over 200 events where plasma drifts exceeded 5 km/s. These drifts, while occurring across all local times, were observed most frequently in the dawn and pre-midnight sectors, predominantly between 64° and 82° invariant latitude. However, some events were detected below 55° invariant latitude, likely linked to SAID phenomena. The study also highlights the seasonal variability of these high-speed flows.

In addition, Martinis et al. (2022) reported SAIDs with velocities reaching at least 10 km/s. Although the Swarm satellites and their electric field instruments, which consist of a pair of Thermal Ion Imagers capable of determining ion drift velocities (Knudsen et al. 2017; Lomidze et al. 2019; Burchill and Knudsen 2022), have been fundamental in recent years for studying the subauroral region, some Swarm observations suggest that these velocities may exceed the upper limits of current instrument capabilities. This raises questions not only about the underlying physical processes but also about the instrumentation challenges faced by future missions seeking to measure such extreme electric fields.

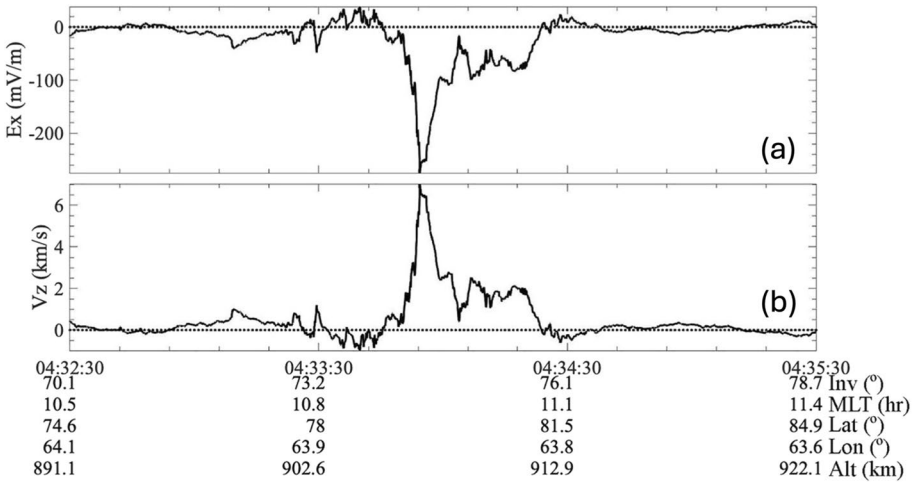

Fig. 3 DE-2 measurements recorded on October 20, 1981: **a** intense electric field and **b** rapid plasma drifts (adapted from Laakso and Pfaff 2023)

Ground-based instruments remain indispensable for understanding the dynamics at mid- and subauroral latitudes. SuperDARN high-frequency (HF) radars, with their extensive coverage at high and mid-latitudes, have proven invaluable in unraveling the dynamics of these regions. The expanding SuperDARN network continues to address measurement gaps, enabling comprehensive global studies (e.g., Nishitani et al. 2019). Numerous investigations have focused on subauroral dynamics (e.g., Oksavik et al. 2006; Makarevich et al. 2011; Kunduri et al. 2012, 2017; Gallardo-Lacourt et al. 2017; Macho et al. 2024). A widely used method to derive plasma convection from SuperDARN line-of-sight data is the spherical harmonic fit technique (Ruohoniemi and Baker 1998). While this method has significantly advanced our understanding of global convection, the spatial and temporal averaging it employs often misses fine-scale features like SAIDs (Kunduri et al. 2017). Recently developed techniques are now capable of capturing finer structures, offering new insights into subauroral dynamics (e.g., Bristow et al. 2022; Nishimura et al. 2024). Despite the extensive coverage and significant advancements provided by SuperDARN measurements, it is important to note that, to avoid aliasing, the maximum measurable SuperDARN velocities depend on the operating frequency and the lag time of the multipulse sequence used. Typical SuperDARN lag times are 2.4 ms, which, depending on the frequency of operation, correspond to a maximum line-of-sight flow velocity of approximately 4 km s^{-1} (Ribeiro et al. 2013). In addition, the refractive index within the SuperDARN scattering region can influence the underestimation of SuperDARN velocity measurements (Gillies et al. 2009).

Incoherent Scatter Radars (ISRs) have also made significant contributions to studying the subauroral ionosphere (e.g., Robinson 2004; Erickson et al. 2011; Aa et al. 2020). While their spatial coverage is more limited compared to SuperDARN, ISRs provide critical measurements of ionospheric properties such as electron density, ion line-of-sight velocity, electron and ion temperatures, and can be used to infer electric fields, composition, and collision frequencies. These measurements can be combined with models to derive additional parameters like ionospheric conductances and neutral winds (e.g., Robinson 2004; Aikio and Selkälä 2009; Nygrén et al. 2011). Understanding these parameters and their temporal evolution is key to unraveling subauroral ionospheric dynamics. However, ISR coverage in North America has diminished in recent years, with existing radars like the Poker Flat ISR often located too far poleward and the Millstone Hill ISR too far equatorward to effectively study the subauroral region. In Europe, the EISCAT radars are also located at auroral latitudes (mainland radars) and in the cusp/polar cap (Svalbard radar), hence not enabling subauroral physics studies.

Similarly, optical instruments have played a pivotal role in understanding the subauroral region. Among these, all-sky imagers (ASIs) have proven invaluable, capturing a wide range of optical emissions at high and mid-latitudes, including the aurora, SAR arcs, STEVE, other forms of continuum emissions (Spanswick et al. 2024), and airglow. In the North American sector, the University of Calgary has been instrumental in deploying and operating ASIs over several decades. One of the most transformative ASI networks is the Time History of Events and Macroscale Interactions during Substorms (THEMIS) All-Sky Imager array. This network, operational since 2005, includes 21 white-light cameras that have revolutionized the observation of the high-latitude ionosphere (Donovan et al. 2006; Mende et al. 2008). The southernmost THEMIS ASI stations provide significant coverage of the subauroral region during moderately active geomagnetic conditions. However, these instruments lack spectral information and photometric calibration. Complementing THEMIS, the Redline Emission Geospace Observatory (REGO) array offers additional capabilities. Comprising nine ASIs, REGO is sensitive to faint auroral emissions

with wavelengths between 628 and 632 nm, peaking at 630.0 nm (Liang et al. 2016). More recently, the Transition Region Explorer (TREx) project has expanded observational capabilities with a suite of advanced instruments, including six blue-light (428 nm) imagers, six near-infrared imagers, seven color (RGB) imagers, and two meridian imaging spectrographs (Liang et al. 2024). On the other hand, in the European sector, most ASIs are found at auroral latitudes, hence optical images of subauroral processes such as STEVE and the picket fence are scarce.

Another type of optical instrument providing crucial measurements in the thermosphere is Fabry Perot interferometers (FPIs), as well as their imaging version known as scanning Doppler imagers (SDIs). These instruments enable the retrieval of neutral wind velocities and temperatures around the altitudes where the measured optical wavelengths have their emission peaks. These correspond to approximately 120 km for the 558 nm line and 250 km for the 630 nm line (e.g., Conde and Smith 1998). Notably, under conditions of weak or absent auroral activity, the green line airglow emission is generally observed near 100 km altitude. However, like for ISRs, FPIs and SDIs are typically installed at auroral (Alaska, northern Fennoscandia, Svalbard) latitudes rather than subauroral latitudes, although during mildly active geomagnetic conditions they have been able to investigate SAPS-associated neutral winds (Conde and Smith 1995; Zou et al. 2022). Installing such instruments at subauroral latitudes could contribute to obtain observations of winds and temperatures in the subauroral thermosphere during moderate and strong geomagnetic storms, a crucial element to help understanding the complex processes occurring in this region.

To address these challenges, a coordinated community effort is essential to expand the coverage of radar and optical instruments in the subauroral zone (e.g., Conde et al. 2023; Gallardo-Lacourt et al. 2023). In the North American sector, significant advancements are on the horizon. The University of Calgary is leading the deployment of a next-generation network of ground-based instruments across Canada through the GDC-Ground (GDC-G) project. This network will include multiple imagers (RGB and red-line), riometers, magnetometers, spectrographs, GNSS receivers, and FPIs, providing an unprecedented suite of ground-based measurements. The initiative is poised to usher in a new era of auroral and subauroral science. Development of the instrumentation is already underway, with deployments planned between 2026 and 2030, and the full network expected to be fully operational by 2030.

In parallel, ongoing developments in Asia, such as the expansion of SuperDARN thanks to the Chinese Dual Auroral Radar Network (CN-DARN) deployment by the National Space Science Center of the Chinese Academy of Sciences (Zhang et al. 2024) as well as the construction of the Sanya tristatic ISR (SYISR) by the Institute of Geology and Geophysics of the Chinese Academy of Sciences (Yue et al. 2024), offer exciting opportunities to enhance global understanding of subauroral dynamics. The integration of complementary instruments—such as satellites, radars, ASIs, and SDIs—within the same observational volume is particularly critical. This coordinated approach enables researchers to disentangle the complex physical processes governing the subauroral ionosphere, particularly during periods of active geomagnetic conditions.

In the Southern Hemisphere, optical observations remain sparse. Within the auroral oval, several stations are equipped with all-sky cameras, including Syowa Station (Japan), McMurdo Station (USA), Dumont d'Urville Station (France), Princess Elisabeth Station (Belgium), and Concordia Station (jointly operated by Italy and France). These stations are primarily located within or near the cusp and auroral oval regions. At subauroral latitudes, optical observations are more limited. While sites in Tasmania and New Zealand provide

some coverage, their geomagnetic latitudes are typically too low to regularly capture subauroral phenomena. Notably, the Australian Antarctic Division camera installed at Macquarie Island (−64° corrected geomagnetic latitude [CGM]) stands out as one of the most valuable assets for monitoring subauroral emissions in the Southern Hemisphere, alongside the Korean-operated camera at King Sejong Station (−48° CGM) in Antarctica.

These advancements, coupled with the application of innovative analysis techniques, are poised to significantly advance the field. By addressing fundamental questions in subauroral research, this collective effort will provide a deeper understanding of the dynamic processes shaping the subauroral region and its interactions with the broader geospace environment.

4 Modeling in the Subauroral Region

4.1 Global Ionosphere–Thermosphere Modeling

First-principle simulations of the ionosphere–thermosphere (IT) system are powerful tools for interpreting observations and exploring physical regimes inaccessible to current instrumentation or direct measurements. However, most models and observational efforts tend to focus on more prominent phenomena at high latitudes or in the equatorial/mid-latitude regions. In contrast, subauroral processes—despite their significance—are often underrepresented.

Several modeling frameworks exist, each with its own strengths and limitations. In this section, we focus on several models which offer valuable capabilities for simulating subauroral dynamics. Combining their respective advantages could help address key open questions in the field.

Global IT models, such as Thermosphere–Ionosphere- Electrodynamics General Circulation Model (TIE-GCM) (Richmond et al. 1992; Solomon et al. 2012; Qian et al. 2014) and Whole Atmosphere Community Climate Model with thermosphere and ionosphere extension (WACCM-X) (Liu et al. 2010, 2018), provide self-consistent simulations of the coupled ionosphere and thermosphere. However, their relatively coarse spatial resolution limits their ability to capture mesoscale structures (tens to hundreds of kilometers in the ionosphere; see (Gabrielse et al. 2023) for a detailed review of mesoscale phenomena). Additionally, their ionospheric modules are often simplified and do not fully capture plasma dynamics along magnetic field lines.

More advanced ionospheric models, such as Sami3 is A Model of the Ionosphere (SAMI3; e.g., Huba and Krall 2013; Huba et al. 2017; Huba and Lu 2024), IRAP Plasmasphere Ionosphere Model (IPIM; e.g., Marchaudon and Blelly 2015, 2020), and Coupled Thermosphere–Ionosphere Plasmasphere Electrodynamics Model (CTIPe; e.g., Millward et al. 2001; Codrescu et al. 2012), offer a more detailed treatment of plasma transport along magnetic field lines, including the effects of solar photoionization and electron precipitation. These models enable simulations with finer resolution (1–5 km) and are particularly suited for studying subauroral phenomena like SAPS and SAR arcs. However, they typically rely on empirical thermospheric inputs (e.g., NRLMSISE Picone et al. 2002; Emmert et al. 2021 and Horizontal Wind Model 14 (HWM14; Drob et al. 2015)) and often lack dedicated modules for simulating optical emissions.

Recent advancements in whole-atmosphere modeling have been crucial for understanding the geospace system as a whole (e.g., Akmaev 2011; Lin et al. 2022; Pham et al. 2022;

Yin et al. 2024, and references therein). As an example, the Multiscale Atmosphere–Geospace Environment (MAGE) model is a coupled geospace model designed to simulate critical mesoscale structures in the geospace system and has been successful in reproducing key aspects of the dynamics observed in the subauroral ionosphere (Lin et al. 2021, 2022; Bao et al. 2023; Lin et al. 2024).

One of the major challenges in accurately modeling subauroral processes is the treatment of electrodynamics in this region. Historically, the subauroral zone has received less attention in both modeling and observations, compared to the auroral oval, polar cap, or equatorial regions. As a result, existing models often treat electrodynamics differently across latitude regions.

In equatorial and mid-latitudes, electrodynamics are often modeled self-consistently, as in TIE-GCM, CTIPe, SAMI3, and soon in IPIM. At high latitudes, electrodynamic inputs are frequently prescribed based on data assimilation products such as Assimilative Mapping of Ionospheric Electrodynamics (AMIE; Richmond 1992; Richmond et al. 1998) and Assimilative Mapping of Geospace Observations (AMGeO; Matsuo 2020; Svaldi et al. 2023, see Fig. 4). However, the transition from high-latitude to subauroral electrodynamics is often handled with ad hoc boundary functions (e.g., the Heppner and Maynard 1987 model), which do not fully capture the complexity of subauroral coupling with the inner magnetosphere.

Recent efforts have proposed empirical convection models tailored to subauroral latitudes to address phenomena like SAPS (Landry and Anderson 2018). Moreover, dedicated models for the inner magnetosphere and its coupling to the ionosphere are beginning to close this gap. These include the Rice Convection Model (RCM) (e.g., Harel et al. 1981; Toffoletto et al. 2003), the Geospace Environment Modeling System for Integrated Studies Ring Current (GEMSIS-RC; e.g., Amano et al. 2011; Yamakawa et al. 2019), and its

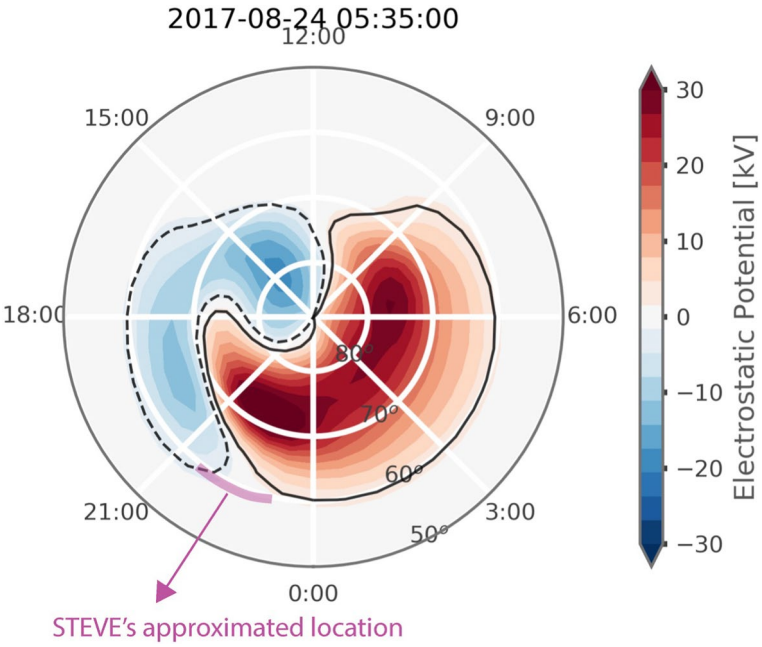

Fig. 4 AMGeO map for a STEVE event occurring on 8 August 2017 (from Svaldi et al. 2023)

coupling with the GEMSIS-POT potential solver (e.g., Nakamizo et al. 2012; Yamakawa et al. 2023). The Comprehensive Inner Magnetosphere–Ionosphere (CIMI) model (Fok et al. 2014, 2024), based on earlier efforts like the Comprehensive Ring Current Model (CRCM; Fok et al. 2001b) and the Radiation Belt Environment (RBE; Fok et al. 2001a), also offers insights into subauroral convection, Region 2 currents, and precipitation patterns. While these models are excellent to describe the electrodynamics between the inner magnetosphere and the ionosphere, they often lack a full physical description of the ionosphere. In this context, the emerging Geospace Environment Model of Ion-Neutral Interactions (GEMINI; e.g., Díaz Peña et al. 2024) presents a promising opportunity. Its flexible, physics-based framework may enables more realistic simulations of subauroral electrodynamics and fine-scale IT interactions (e.g., Lynch et al. 2022).

4.2 Light Emissions Modeling

Some ionospheric models focus specifically on kinetic processes by solving field-aligned transport equations for suprathermal electrons in a time-independent framework. These models aim to assess how energy degradation, ion production, and optical emissions develop along magnetic field lines, without accounting for the dynamics of the thermal ionospheric plasma.

Notable examples in this category include the Transsolo model (e.g., Lummerzheim and Lilensten 1994; Robert et al. 2023) and Global Airglow (GLOW; e.g., Solomon et al. 1988; Solomon 2017). GLOW uses a simplified approach with two electron streams, while the current version of the Transsolo model allows for more detailed modeling with 16 or 32 electron streams. Both models compute emissions based on sets of electron collision cross sections with the main atmospheric species across relevant altitudes. In addition to auroral emissions, they can also simulate dayglow effects driven by solar EUV radiation.

However, a subset of auroral and airglow emissions originate from forbidden transitions under the electric dipole approximation. These transitions involve metastable excited states with long lifetimes—up to 110 s for the O I 630 nm red line, and up to 9.95 h for the N I 520 nm line. The subsequent de-excitation of these states is governed by a complex network of chemical and ion reactions, highly dependent on the local thermodynamic conditions (i.e., neutral, ion, and electron temperatures) in the ionosphere–thermosphere system. At auroral regions, additional optical signatures appear, including strong molecular bands such as the N2 First and Second Positive systems, and the Vegard–Kaplan (VK) band in the visible and near-UV range. Recent work by Barthelemy et al. (2025) has extended Transsolo to produce synthetic auroral spectra, cataloging a broad range of visible emission lines and bands.

Understanding the drivers of subauroral emissions is essential for interpreting and modeling these features accurately. In the case of thermally excited emissions, the excitation thresholds play a central role. For instance, the O I red line (630.0 nm) has a threshold energy of 1.96 eV, corresponding to an equivalent temperature of about 22,700 K. While such high temperatures are uncommon, the high-energy tail of a Maxwellian distribution can populate these states even at lower average temperatures.

More energetic transitions–such as the O I green line at 557.7 nm (threshold 4.19 eV) or the N2 VK band (threshold ~6.17 eV)—are less likely to be excited thermally. Their absence, especially in Stable Auroral Red (SAR) arcs, suggests a dominance of low-energy electron impacts, elevated temperatures, or temperature-sensitive chemical processes (e.g., Solomon et al. 1988). Conversely, the presence of high-threshold emissions such as $N2^+$ bands at 391

nm and 428 nm (threshold ~18.75 eV) typically signals the involvement of suprathermal electron precipitation, as seen in traditional auroral zones.

To realistically simulate subauroral optical structures, models must incorporate temperature-dependent chemistry, flexible atmospheric composition, and possibly locally enhanced temperature profiles at select altitudes. Standard atmospheric and ionospheric models may underestimate or misrepresent the densities of key species under these perturbed conditions. Numerically, this presents additional challenges: sharp gradients or poorly defined boundaries between disturbed and undisturbed regions can induce instabilities in simulations, underscoring the need for adaptable and robust modeling frameworks.

4.3 Progress in Subauroral Modeling

A key step toward improving the modeling of auroral and subauroral processes is the incorporation of more realistic thermospheric inputs into ionospheric models such as SAMI3 and IPIM. The thermosphere responds strongly to intense electric fields associated with phenomena like SAPS and STEVE, as well as to inner magnetospheric heat fluxes that drive SAR arcs. One promising avenue is the one-way coupling of general circulation models like TIE-GCM or WACCM-X with SAMI3, which has shown potential for enhancing ionospheric representation, particularly at equatorial and mid-latitudes (Huba et al. 2017; Huba and Lu 2024). However, this coupling is currently unidirectional—SAMI3 receives thermospheric inputs from TIE-GCM or WACCM-X, but does not provide feedback, meaning the thermospheric response to ionospheric dynamics remains unmodeled.

Another promising direction is the coupling of ionospheric models with light emission models. This would not only allow for a detailed representation of ionospheric dynamics, but also enable the generation of synthetic spectra of auroral and subauroral emissions. An example of this effort is the ongoing integration between IPIM and Transsolo, which builds on the foundation laid by the earlier TRANSCAR model (Lilensten and Blelly 2002; Blelly et al. 2005), the precursor to IPIM. Assimilating observational data—such as subauroral convection fields from SuperDARN—into these coupled frameworks could greatly improve our understanding of emission mechanisms in features such as SAR arcs and STEVE.

The ultimate goal is a fully coupled system integrating thermospheric, ionospheric, and electrodynamic models with a light emission module. While technically ambitious, this approach holds the greatest potential for accurately reproducing subauroral dynamics and emissions. Some progress has already been made in this direction. For example, Lin et al. (2024) modeled SAR arcs using a TIE-GCM–CIMI coupling, and more comprehensive frameworks like the Multiscale Atmosphere-Geospace Environment (MAGE) model have begun to explore SAPS dynamics using multi-model associations (Lin et al. 2021; Bao et al. 2023).

In parallel, efforts are underway to develop high-resolution, localized models tailored to subauroral studies, as exemplified by the work of Liang et al. (2021, 2022). These models offer a more targeted approach that can complement global simulations and support future integration efforts.

5 The Chemistry in the Subauroral Region

It is important to begin by noting that each subauroral emission type has a distinct chemistry, which can be investigated through the intensity of its characteristic emission lines. Many numerical simulations either include or can be coupled with chemistry modules. However, one major challenge lies in the poorly constrained thermodynamic conditions of subauroral regions. This uncertainty is particularly critical for forbidden emission lines—such as the O I red and green lines.

SAR arcs are primarily composed of emissions from the O I 630.0 nm red line ($O(^1D) \rightarrow O(^3P)$). While the underlying chemistry is similar to the reaction set described by Solomon et al. (1988), the differing thermal conditions in subauroral regions significantly alter the reaction rates (e.g., Kozyra et al. 1997; Sazykin et al. 2002). The chemistry becomes even more complex in the case of STEVE, where extreme SAIDs are observed, along with a continuum component as discussed in Harding et al. (2020). Nishimura et al. (2023) provide a comprehensive review of the unresolved questions surrounding STEVE emissions, including the associated chemistry.

Mishin (2023) suggests that suprathermal electrons with relatively low energies are necessary to explain the occurrence of STEVE and picket fence structures, particularly in the absence of the N_2^+ 428 nm emission line and the simultaneous presence of the first positive band. Both this study and Liang and Donovan (2024) highlight the importance of vibrationally excited N_2 in producing STEVE-like emissions. However, Liang and Donovan (2024) emphasize that while vibrational energy transfer driven by SAID plays a critical role in exciting N_2, it is insufficient to populate the high vibrational levels to the concentrations required by the emission models proposed by Harding et al. (2020). As a result, the generation mechanism behind STEVE emissions remains one of the most debated topics in aeronomy. Additionally, STEVE events exhibit a continuum emission, the origin of which remains poorly understood. An important unresolved question concerns the potential association of this continuum emission with NO_2, as originally proposed by Gillies et al. (2019) and subsequently examined by Harding et al. (2020).

High-resolution spectral measurements are critical for identifying fine spectral features that may be attributable to NO_2. Laboratory spectra obtained from laser-induced fluorescence experiments offer a valuable basis for comparison. In particular, high-resolution molecular band data in the red spectral region, as presented in Smalley et al. (1975) and Delon et al. (1991), can serve as important references. Comparing these laboratory spectra with observations from subauroral latitudes could help elucidate the origin of the observed continuum emissions. In this context, the recently reported subauroral continuum spectra at high latitudes by Partamies et al. (2024) represent a promising step forward in understanding the mechanisms responsible for continuum emissions in the subauroral region.

Additionally, Wang et al. (2012) studied the effects of SAPS on subauroral thermospheric chemistry using the TIE-GCM model. Their simulations showed that SAPS-induced thermospheric heating causes atmospheric upwelling, increasing the molecular-to-atomic ratio in the subauroral thermosphere. These composition changes enhance electron recombination, leading to reduced electron densities. Similar mechanisms have been proposed to explain F-region electron density depletion at both auroral and subauroral latitudes, driven by heating and composition changes due to molecular upwelling (Grandin et al. 2015; Marchaudon et al. 2018; Geethakumari et al. 2024).

One major source of uncertainty in modeling subauroral chemistry is the lack of *in situ* measurements of ion–neutral collision frequencies and cross sections (see Sections 4.4

and 4.5 in Palmroth et al. 2021). Values used in numerical models are often extrapolated from laboratory-derived formulas (e.g., Banks 1966; Woo and Wong 1971), sometimes beyond their valid regimes. Despite these limitations, insights from heliophysics and other related fields may prove valuable. For example, while most existing formulas for distribution-averaged momentum transfer rates and collisional frequencies in the ionosphere assume a Maxwellian distribution, St-Maurice and Schunk (1979) and Goodwin et al. (2018) discuss the potential for non-Maxwellian ion distributions under strong electric fields. Furthermore, studies of meteoroid atmospheric entry—particularly during Leonid meteor showers—face similar uncertainties. Leonids enter Earth's atmosphere at speeds up to 70 km/s, far exceeding SAID speeds (~7 km/s), leading to energetic interactions. For instance, an iron atom at 70 km/s carries ~1.5 keV of kinetic energy, while at 7 km/s this drops to ~15 eV. Though SAID particles may not be iron, this analogy offers a rough estimate of the energy range relevant for excitation processes. Substituting iron with oxygen (O) atoms or ions further reduces the expected energy to a few eV, which is still within the range necessary for significant collisional excitation of the background atmosphere. The literature on collisional cross sections shows general trends that can be extrapolated across species (e.g., Ishimoto et al. 1994). The Bethe theory of stopping power offers another perspective: it suggests that the collisional cross section of a heavy ion can be approximated by scaling the electron impact cross section (e.g., Salvat et al. 2022). For instance, if electron collisions peak near 50 eV, equivalent proton impact collisions would peak around 100 keV due to the ~2000x mass difference (e.g., De Heer et al. 1966). While these approximations do not replace direct measurements, they may offer useful constraints for modeling and help illuminate the underlying chemistry of the subauroral ionosphere.

6 Needed Experiments and Mission: Current and Future Initiatives

One of the main challenges in studying the subauroral region is the limited availability of measurements, especially in situ observations between 100 and 400 km altitude, where many phenomena discussed in Sect. 2 occur. This section highlights several missions and initiatives that promise to significantly advance our understanding of this critical region.

Among the most anticipated missions in the U.S. is NASA's Geospace Dynamics Constellation (GDC), recommended in the 2013 and 2024 USA Heliophysics Decadal Surveys as a high priority. GDC will deploy six identical satellites equipped with state-of-the-art instruments, including a Langmuir probe (AETHER), electrostatic analyzers (CAPE), a mass spectrometer (MoSAIC), a magnetometer (NEMESIS), a thermal plasma sensor (TPS), and a radio occultation probe (ProFILE). Operating at altitudes between 350–400 km, GDC will provide high-cadence, global-scale measurements, transforming our understanding of aeronomy and subauroral dynamics. Coordination with ground-based observations and other missions will amplify the scientific returns of GDC, establishing it as a community-driven mission. Importantly, one of the key science objectives of GDC is to unveil several fundamental aspects of subauroral dynamics.

Also prioritized in the 2013 and 2024 Decadal Surveys is NASA's Dynamical Neutral Atmosphere–Ionosphere Coupling (DYNAMIC) mission, which will investigate how the lower atmosphere influences the upper atmosphere, particularly in the 80–200 km altitude range. By deploying multiple spacecraft, DYNAMIC will enable simultaneous measurements from various locations, revealing how atmospheric waves propagate and

interact. Synergistic observations between GDC and DYNAMIC will provide a comprehensive understanding of atmospheric coupling and its impact on the near-Earth space environment.

In Europe, ESA's Daedalus mission study was conceived to address critical knowledge gaps in the upper atmosphere (Sarris et al. 2020; Palmroth et al. 2021). As part of ESA's Earth Explorer 10 pre-feasibility studies, Daedalus proposed an innovative mission design that included in situ measurements of a large number of physical parameters (including electric and magnetic fields, ion and neutral composition and density, temperatures, particle fluxes) down to 120 km altitude. The mission study aimed to quantify energy deposition via Joule heating and particle precipitation, significantly reducing uncertainties in existing models. While Daedalus was not retained by ESA at the end of Phase-0, the ESA-NASA Lower Thermosphere–Ionosphere Science (ENLoTIS) Working Group was established in 2022 to explore new mission concepts targeting the 100–200 km altitude range, building on the work achieved during the Daedalus pre-feasibility study. As part of ESA's Space Situational Awareness – Space Weather (S2P) program, the Aurora-D (Demonstration) and Aurora-C (Constellation) missions are designed to capture images of auroral activity using the Wide Field Auroral Imager (WFAI) instrument. These missions will operate in high-altitude (~6500 km), quasi-polar orbits. The WFAI instrument consists of two modules: one operating in the far ultraviolet (FUV), known as AUI, and the other in the visible spectrum, known as AOSI. The visible module is a spectro-imager designed to observe auroral emissions in the 380–900 nm range, with a spatial resolution of approximately 30 km at ground level. With a large field of view (57° × 57°), the instrument has the potential to capture subauroral features in addition to the main auroral oval. The combined coverage of visible and FUV emissions will enable the differentiation between particle precipitation and thermal effects, contributing to a better understanding of auroral and subauroral processes. Aurora-D is scheduled for launch in 2029, with the Aurora-C constellation mission planned for 2033. Importantly, synergy between these space-based observations and coordinated ground-based optical measurements will be crucial for reconstructing the three-dimensional structure and full geometry of subauroral emissions. These efforts underscore the importance of detailed in situ measurements to unravel the dynamics of neutral–ion interactions and space weather processes in this underexplored region.

The Antarctic Geospace and Atmosphere Research (AGATA) program (Alfonsi et al. 2023), part of the Scientific Committee on Antarctic Research (SCAR), focuses on monitoring and understanding Sun-Earth interactions in polar regions. AGATA also investigates how polar phenomena influence lower latitudes, including subauroral regions, offering critical insights into global geospace dynamics.

Citizen science initiatives have proved invaluable in understanding auroral and subauroral dynamics. Several projects, such as Aurorasaurus (https://doi.org/https://www.aurorasaurus.org/) and Skywarden (https://doi.org/https://www.taivaanvahti.fi/), facilitate the collection of auroral observations made by aurora chasers. These observations can include images and the identification of specific optical emission forms including those that are typical of the subauroral region, such as SAR arcs, STEVE, and the dunes. More recently, the ARCTICS (Auroral Research Coordination: Towards Internationalised Citizen Science) working group, supported by the International Space Science Institute in Bern, brings together experts and citizen scientists to investigate unexplained optical phenomena in the dark sky. The ARCTICS collaborators analyze events from citizen science photographs in conjunction with ground-based and satellite measurements. By specifically inviting citizen scientists, many of whom live at subauroral latitudes, to contribute to scientific research, a wealth of additional observations can be expected, that can contribute to bridge the gaps

in science-grade optical data (see Sect. 3). To this aim, ARCTICS recently issued a set of open-access documents to facilitate citizen science collaboration in auroral and subauroral studies (Herlingshaw et al. 2024). A detailed review of the role of citizen science in heliophysics, particularly in subauroral studies, can be found in Grandin et al. (2025, this issue).

These missions and initiatives exemplify the growing international effort to address the challenges of studying the subauroral region. By combining cutting-edge technology, ground-based and satellite observations, and citizen science, these endeavors will undoubtedly expand our understanding of the complex interactions between Earth's atmosphere and space.

7 Concluding Remarks and Open Questions in Subauroral Research

Numerous unresolved questions persist within the field of subauroral science, presenting opportunities for targeted investigation by the scientific community over the coming years. This section highlights some of the most pressing issues that demand attention to advance our understanding of subauroral dynamics.

One critical area of inquiry involves the mechanisms responsible for generating the continuum emissions observed during STEVE events. Despite substantial efforts to model the physical and chemical processes involved (e.g., Harding et al. 2020; Mishin 2023; Liang and Donovan 2024), the exact origins remain unknown. Understanding how extreme SAID events trigger the continuum spectrum associated with STEVE, along with the subauroral ionosphere's changing chemistry between altitudes of 200–400 km, would provide valuable insights. Such understanding could also illuminate continuum emissions in other regions, such as the auroral oval and higher latitudes (e.g., Spanswick et al. 2024; Partamies et al. 2024). While the mechanisms may vary across scenarios, identifying common constraints would refine our understanding of continuum emission generation. Progress in this area will require a combination of theoretical modeling, remote sensing, and in situ measurements to untangle the complex physics and chemistry at play.

At a fundamental level, the physical drivers of extreme SAIDs observed during STEVE events remain poorly understood. The SAID velocities associated with STEVE (>3 km/s) far exceed the typical values cited in the literature (e.g., Puhl-Quinn et al. 2007; Knudsen et al. 2017), raising scientific and technological challenges. These extreme SAIDs not only demand an explanation regarding their underlying physics but also challenge the capabilities of existing instrumentation for in situ and remote sensing observations. Although SAIDs have been well documented during the substorm recovery phase (e.g., Anderson et al. 1991, 1993, 2001; Foster et al. 1994; Galperin 2002; He et al. 2014), their precise mechanisms and coupled magnetospheric, ionospheric, and thermospheric dynamics involved remain contentious (e.g., Mishin 2013, 2023; Nishimura et al. 2023). Adding to this complexity, recent observations of STEVE and extreme SAIDs during geomagnetically quiet conditions (Gallardo-Lacourt et al. 2024) raise new questions about solar wind–magnetosphere–ionosphere–thermosphere coupling. A study by Nishimura et al. (2024) has identified unusual characteristics during such events, including extended plasmapause boundaries, electron-dominated injections at geosynchronous orbit, and exceptionally low electron temperatures. These findings underscore the need for simulation-driven investigations to capture the intricate coupling mechanisms across the MIT system.

Another significant challenge lies in understanding the transition between STEVE and SAR arcs (e.g., Martinis et al. 2022; Gillies et al. 2023). Outstanding issues include

whether SAR arcs persist behind or at higher altitudes relative to bright STEVEs, and the extent to which SAR arcs contribute to STEVE formation. Some SAR arcs appear to evolve into STEVEs, while others do not, and in some cases, STEVEs seem to revert back into SAR arcs. These observations suggest complex interactions between the ring current and the ionosphere that are not yet fully understood. In certain events, SAR arcs observed during transitions are brighter than typical SAR arcs, raising further questions about the underlying processes. Additionally, the subauroral ionosphere undergoes rapid, minute-scale modifications during these transitions, the drivers of which remain poorly characterized.

The enigmatic structures associated with STEVE, known as the Picket Fence (see Sect. 2), present another set of unanswered questions. Due to their small-scale size, current instruments often struggle to capture these features, making citizen science contributions invaluable. Despite these efforts, fundamental aspects remain unclear. The physical mechanism responsible for forming the Picket Fence and the source of its green emission are not well understood. While Nishimura et al. (2019) suggested particle precipitation as a possible driver, Mende et al. (2019) noted that the observed spectrum did not align with the typical green line emissions produced by precipitation. Gasque et al. (2023), using kinetic calculations, proposed that low-altitude parallel electric fields could accelerate local thermal electrons to replicate the Picket Fence spectra without requiring particle precipitation. Despite considerable instrumental and logistical challenges, acquiring measurements of these parallel electric fields and detailed observations of the subauroral region at the altitude of the Picket Fence (~110 km) is essential. Such data would offer valuable insights into the fundamental physics driving the generation of the Picket Fence phenomenon.

Additionally, the relationship between STEVE and the Picket Fence is poorly understood. It is unclear at what stage in STEVE's evolution the Picket Fence appears, whether it occurs equatorward or poleward, and why some STEVE events are accompanied by the Picket Fence while others are not. The role of STEVE in driving Picket Fence characteristics and its potential relationship to other subauroral structures, such as the streaks (Semeter et al. 2020) or Fragmented Auroral-like Emissions (FAEs; Dreyer et al. 2021; Whiter et al. 2021), remains speculative. Detailed data analysis and modeling comparisons could shed light on these phenomena.

Other optical emission forms typical of the subauroral region also remain largely elusive and would require further investigation. In the case of the dune aurora, additional evidence is needed to conclude whether the wave-like pattern in the diffuse emission is indeed associated with the presence of an atmospheric wave which modulates spatially the neutral density, or if alternative hypotheses placing the origin of the dunes' morphology in the magnetosphere (e.g., He et al. 2023) are confirmed. Addressing this question requires finding dune events for which ground-based observations can be supplemented by conjugate satellite data in the magnetosphere and in low-Earth orbit. In addition, it is unclear whether the auroral emission in the dunes is related to proton precipitation or if the presence of strong precipitating proton fluxes during the event studied by Grandin et al. (2021) was merely coincidental. Measuring the dunes' optical emission spectra and interpreting them with the aid of kinetic transport models such as Transsolo or GLOW could provide insight into this question. More generally, modeling studies are needed to refine our understanding of the optical emission mechanisms associated with subauroral phenomena, especially those that involve secondary electrons associated with auroral proton precipitation (e.g., RAGDA and IPA).

Finally, addressing the broader dynamics of subauroral regions requires understanding the coupling between the magnetosphere, ionosphere, and thermosphere. Key questions include the generation and propagation of atmospheric waves, the role of neutral winds,

and the timescales over which these processes influence subauroral dynamics. Investigating how atmospheric composition modifies the region and impacts system-level interactions will further enhance our knowledge of subauroral science.

Acknowledgements The authors gratefully acknowledge the International Space Science Institute (ISSI) for organizing the workshop on Physical Links Between Weather and Climate in Space and the Lower Atmosphere at ISSI Bern (Switzerland) on 22–26 January 2024. This article is one of the outputs from the workshop. BGL would like to thank Dr. Reza Janalizadeh and Dr. Bharat Kunduri for the insightful discussions that helped improve this paper. The authors would like to thank Jeremy Kuzub and Pirjo Koski for kindly allowing the use of their STEVE and Dunes photographs, respectively, in Figure 2. BGL is supported by the NASA Mesoscale Magnetospheric Dynamics—Heliophysics Internal Science Funding Model (HISFM). MG acknowledges funding from the Research Council of Finland (grant 360433-ANAON) and from the European Research Council (Starting Grant 101161971-LOUARN). AM and MB are supported by Centre National de la Recherche Scientifique (CNRS) through the Action Thématique Soleil-Terre of the Institut National Terre et Univers (ATST/INSU) and Centre National d'Etudes Spatiales (CNES).

Declarations

Conflict of interest MG is Guest Editor of the Special Issue to which this article is submitted.

References

Aa E, Erickson PJ, Zhang S-R, Zou S, Coster AJ, Goncharenko LP, Foster JC (2020) A statistical study of the subauroral polarization stream over north american sector using the millstone hill incoherent scatter radar 1979–2019 measurements. J Geophys Res Space Phys 125(10):028584. https://doi.org/10.1029/2020JA028584

Aikio AT, Selkälä A (2009) Statistical properties of Joule heating rate, electric field and conductances at high latitudes. Ann Geophys 27(7):2661–2673. https://doi.org/10.5194/angeo-27-2661-2009

Akmaev RA (2011) Whole atmosphere modeling: connecting terrestrial and space weather. Rev Geophys 49(4):1 (**10.1029/2011RG000364**)

Alfonsi L, Bergeot N, Miloch WJ (2023) AGATA-a new SCAR programme planning group. In: AGU fall meeting abstracts, vol 2023, pp 24–03

Amano T, Seki K, Miyoshi Y, Umeda T, Matsumoto Y, Ebihara Y, Saito S (2011) Self-consistent kinetic numerical simulation model for ring current particles in the earth's inner magnetosphere. J Geophys Res Space Phys 116(2):234. https://doi.org/10.1029/2010JA015682

Anderson PC, Heelis RA, Hanson WB (1991) The ionospheric signatures of rapid subauroral ion drifts. J Geophys Res Space Phys 96(A4):5785–5792. https://doi.org/10.1029/90JA02651

Anderson BJ, Erlandson RE, Zanetti LJ (1992) A statistical study of Pc 1–2 magnetic pulsations in the equatorial magnetosphere: 1. Equatorial occurrence distributions. J Geophys Res Space Phys 97(3A):3075–3088. https://doi.org/10.1029/91JA02706

Anderson PC, Hanson WB, Heelis RA, Craven JD, Baker DN, Frank LA (1993) A proposed production model of rapid subauroral ion drifts and their relationship to substorm evolution. J Geophys Res Space Phys 98(A4):6069–6078. https://doi.org/10.1029/92JA01975

Anderson PC, Carpenter DL, Tsuruda K, Mukai T, Rich FJ (2001) Multisatellite observations of rapid subauroral ion drifts (said). J Geophys Res Space Phys 106(A12):29585–29599. https://doi.org/10.1029/2001JA000128

Anger CD, Moshupi MC, Wallis DD, Murphree JS, Brace LH, Shepherd GG (1978) Detached auroral arcs in the trough region. J Geophys Res Space Phys 83(A6):2683–2689. https://doi.org/10.1029/JA083iA06p02683

Archer WE, Gallardo-Lacourt B, Perry GW, St-Maurice JP, Buchert SC, Donovan E (2019) Steve: the optical signature of intense subauroral ion drifts. Geophys Res Lett 46(12):6279–6286. https://doi.org/10.1029/2019GL082687

Archer WE, Maurice JPS, Gallardo-Lacourt B, Perry GW, Cully CM, Donovan E, Gillies DM, Downie R, Smith J, Eurich D (2019) The vertical distribution of the optical emissions of a Steve and picket fence event. Geophys Res Lett 46(19):10719–10725. https://doi.org/10.1029/2019GL084473

Banks P (1966) Collision frequencies and energy transfer. Ions Planet Space Sci 14(11):1105–1122. https://doi.org/10.1016/0032-0633(66)90025-0

Bao S, Wang W, Sorathia K, Merkin V, Toffoletto F, Lin D, Pham K, Garretson J, Wiltberger M, Lyon J, Michael A (2023) The relation among the ring current, subauroral polarization stream, and the geospace plume: MAGE simulation of the 31 march 2001 super storm. J Geophys Res Space Phys 128(12):031923. https://doi.org/10.1029/2023JA031923

Barthelemy M, Robert E, Lamy H (2025) Synthetic spectra of the aurora. J Space Weather Space Clim. https://doi.org/10.1051/swsc/2025013

Blelly P-L, Lathuillère C, Emery B, Lilensten J, Fontanari J, Alcaydé D (2005) An extended TRANSCAR model including ionospheric convection: simulation of EISCAT observations using inputs from AMIE. Ann Geophys 23(2):419–431. https://doi.org/10.5194/angeo-23-419-2005

Bristow WA, Lyons LR, Nishimura Y, Shepherd SG, Donovan EF (2022) High-latitude plasma convection based on superdarn observations and the locally divergence free criterion. J Geophys Res Space Phys 127(12):2022–030883. https://doi.org/10.1029/2022JA030883

Burchill JK, Knudsen DJ (2022) Swarm thermal ion imager measurement performance. Earth Planets Space 74(1):1880–5981. https://doi.org/10.1186/s40623-022-01736-w

Codrescu MV, Negrea C, Fedrizzi M, Fuller-Rowell TJ, Dobin A, Jakowsky N, Khalsa H, Matsuo T, Maruyama N (2012) A real-time run of the coupled thermosphere ionosphere plasmasphere electrodynamics (CTIPe) model. Space Weather. https://doi.org/10.1029/2011SW000736

Conde M, Smith RW (1995) Mapping thermospheric winds in the auroral zone. Geophys Res Lett 22(22):3019–3022. https://doi.org/10.1029/95GL02437

Conde M, Smith RW (1998) Spatial structure in the thermospheric horizontal wind above Poker Flat, Alaska, during solar minimum. J Geophys Res Space Phys 103(A5):9449–9471. https://doi.org/10.1029/97JA03331

Conde M, Hampton D, Thorsen D, Ridley A, Bristow W, Harding B, Dhadly M, Mesquita R, Dandenault P, Banks F, Makela J, Bhatt A, Kendall E, Taylor M, Martinis C, Rideout W, Chau J, Datta-Barua S, Donovan E, Spanswick E (2023) The need for a large-scale dense array of ground based observatories to monitor thermospheric and space weather. Bull AAS 55(3)

Craven JD, Frank LA, Ackerson KL (1982) Global observations of a SAR arc. Geophys Res Lett 9(9):961–964. https://doi.org/10.1029/GL009i009p00961

De Heer FJ, Schutten J, Moustafa H (1966) Ionization and electron capture cross sections for protons incident on noble and diatomic gases between 10 and 140 keV. Physica 32(10):1766–1792. https://doi.org/10.1016/0031-8914(66)90091-7

Delon A, Jost R, Lombardi M (1991) NO2 jet cooled visible excitation spectrum: Vibronic chaos induced by the $\tilde{X}^2A_1$—$\tilde{A}^2B_2$ interaction. J Chem Phys 95(8):5701–5718. https://doi.org/10.1063/1.461620

Dewan EM, Picard RH (1998) Mesospheric bores. J Geophys Res 103(D6):6295–6306. https://doi.org/10.1029/97JD02498

Dewan EM, Picard RH (2001) On the origin of mesospheric bores. J Geophys Res 106(D3):2921–2927. https://doi.org/10.1029/2000JD900697

Díaz Peña J, Zettergren M, Semeter J, Nishimura Y, Hirsch M, Walsh BM (2024) 3D simulation of an extreme SAID flow channel. J Geophys Res Space Phys 129(6):032660. https://doi.org/10.1029/2024JA032660

Donovan E, Mende S, Jackel B, Frey H, Syrjäsuo M, Voronkov I, Trondsen T, Peticolas L, Angelopoulos V, Harris S, Greffen M, Connors M (2006) The THEMIS all-sky imaging array-system design and initial results from the prototype imager. J Atmos Solar Terr Phys 68(13):1472–1487. https://doi.org/10.1016/j.jastp.2005.03.027

Dreyer J, Partamies N, Whiter D, Ellingsen PG, Baddeley L, Buchert SC (2021) Characteristics of fragmented aurora-like emissions (FAEs) observed on Svalbard. Ann Geophys 39(2):277–288. https://doi.org/10.5194/angeo-39-277-2021

Drob DP, Emmert JT, Meriwether JW, Makela JJ, Doornbos E, Conde M, Hernandez G, Noto J, Zawdie KA, McDonald SE, Huba JD, Klenzing JH (2015) An update to the horizontal wind model (HWM): the quiet time thermosphere. Earth Space Sci 2(7):301–319. https://doi.org/10.1002/2014EA000089

Eather RH (1968) Spectral intensity ratios in proton-induced auroras (1896-1977). J Geophys Res 73(1):119–125. https://doi.org/10.1029/JA073i001p00119

Emmert JT, Drob DP, Picone JM, Siskind DE, Jones M Jr, Mlynczak MG, Bernath PF, Chu X, Doornbos E, Funke B, Goncharenko LP, Hervig ME, Schwartz MJ, Sheese PE, Vargas F, Williams BP, Yuan T (2021) NRLMSIS 2.0: a whole-atmosphere empirical model of temperature and neutral species densities. Earth Space Sci 8(3):001321. https://doi.org/10.1029/2020EA001321

Erickson PJ, Beroz F, Miskin MZ (2011) Statistical characterization of the American sector subauroral polarization stream using incoherent scatter radar. J Geophys Res Space Phys. https://doi.org/10.1029/2010JA015738

Fok M-C, Kozyra JU, Brace LH (1991) Solar cycle variation in the subauroral electron temperature enhancement: comparison of AE-C and DE 2 satellite observations. J Geophys Res Space Phys 96(A2):1861–1866. https://doi.org/10.1029/90JA02377

Fok M-C, Kozyra JU, Nagy AF, Rasmussen CE, Khazanov GV (1993) Decay of equatorial ring current ions and associated aeronomical consequences. J Geophys Res Space Phys 98(A11):19381–19393. https://doi.org/10.1029/93JA01848

Fok M-C, Moore TE, Spjeldvik WN (2001) Rapid enhancement of radiation belt electron fluxes due to substorm dipolarization of the geomagnetic field. J Geophys Res Space Phys 106(A3):3873–3881. https://doi.org/10.1029/2000JA000150

Fok M-C, Wolf RA, Spiro RW, Moore TE (2001) Comprehensive computational model of Earth's ring current. J Geophys Res Space Phys 106(A5):8417–8424. https://doi.org/10.1029/2000JA000235

Fok M-C, Buzulukova NY, Chen S-H, Glocer A, Nagai T, Valek P, Perez JD (2014) The comprehensive inner magnetosphere-ionosphere model. J Geophys Res Space Phys 119(9):7522–7540. https://doi.org/10.1002/2014JA020239

Fok M-C, Wolf RA, Ferradas CP, Kang S-B, Glocer A, Buzulukova NY, Ma Q, Welling DT (2024) Implementation of an asymmetric internal field in the comprehensive inner magnetosphere-ionosphere (CIMI) model. J Geophys Res Space Phys 129(12):033075. https://doi.org/10.1029/2024JA033075

Foster JC, Burke WJ (2002) SAPS: a new categorization for sub-auroral electric fields. EOS Trans Am Geophys Union 83(36):393–394. https://doi.org/10.1029/2002EO000289

Foster JC, Buonsanto MJ, Mendillo M, Nottingham D, Rich FJ, Denig W (1994) Coordinated stable auroral red arc observations: Relationship to plasma convection. J Geophys Res Space Phys 99(A6):11429–11439. https://doi.org/10.1029/93JA03140

Gabrielse C, Gkioulidou M, Merkin S, Malaspina D, Turner DL, Chen MW, Ohtani S-I, Nishimura Y, Liu J, Birn J, Deng Y, Runov A, McPherron RL, Keesee A, Yin Lui AT, Sheng C, Hudson M, Gallardo-Lacourt B, Angelopoulos V, Lyons L, Wang C-P, Spanswick EL, Donovan E, Kaeppler SR, Sorathia K, Kepko L, Zou S (2023) Mesoscale phenomena and their contribution to the global response: a focus on the magnetotail transition region and magnetosphere-ionosphere coupling. Front Astron Space Sci 10:1151339. https://doi.org/10.3389/fspas.2023.1151339

Galand M (2001) Introduction to special section: proton precipitation into the atmosphere. J Geophys Res 106:1–6. https://doi.org/10.1029/2000JA002015

Galand M, Chakrabarti S (2006) Proton aurora observed from the ground. J Atmos Solar Terr Phys 68(13):1488–1501. https://doi.org/10.1016/j.jastp.2005.04.013

Gallardo-Lacourt B, Nishimura Y, Lyons LR, Mishin EV, Ruohoniemi JM, Donovan EF, Angelopoulos V, Nishitani N (2017) Influence of auroral streamers on rapid evolution of ionospheric SAPS flows. J Geophys Res Space Phys 122(12):12406–12420. https://doi.org/10.1002/2017JA024198

Gallardo-Lacourt B, Nishimura Y, Donovan E, Gillies DM, Perry GW, Archer WE, Nava OA, Spanswick EL (2018) A statistical analysis of STEVE. J Geophys Res Space Phys 123(11):9893–9905. https://doi.org/10.1029/2018JA025368

Gallardo-Lacourt B, Frey HU, Martinis C (2021) Proton aurora and optical emissions in the subauroral region. Space Sci Rev 217(1):10. https://doi.org/10.1007/s11214-020-00776-6

Gallardo-Lacourt B, Perry G, Kunduri B, Martinis C, Halford A, Gillies DM, Zettergren M, Ledvina V, Thomas E, Grandin M, Brandt L, Lejosne S, Lyons L, Svaldi V, Goodwin L, Kosar B, Maruyama N, MacDonald E, Harding B, Rowland D, Nishimura T, Hunnekuhl M, Archer W, Anderson P, Donovan E (2023) The importance of extreme dynamic signatures in the sub-auroral region. Bull AAS 55(3)

Gallardo-Lacourt B, Nishimura Y, Kepko L, Spanswick EL, Gillies DM, Knudsen DJ, Burchill JK, Skone SH, Pinto VA, Chaddock D, Kuzub J, Donovan EF (2024) Unexpected STEVE observations

at high latitude during quiet geomagnetic conditions. Geophys Res Lett 51(19):110568. https://doi.org/10.1029/2024GL110568

Galperin YI (2002) Polarization jet: characteristics and a model. Ann Geophys 20(3):391–404. https://doi.org/10.5194/angeo-20-391-2002

Gasque LC, Janalizadeh R, Harding BJ, Yonker JD, Gillies DM (2023) It's not easy being green: kinetic modeling of the emission spectrum observed in STEVE's picket fence. Geophys Res Lett 50(21):106073. https://doi.org/10.1029/2023GL106073

Geethakumari GP, Aikio AT, Cai L, Vanhamäki H, Virtanen II, Coster A, Marchaudon A, Blelly P-L, Maute A, Norberg J, Oyama S, Zhang Y, Kunduri BSR (2024) Total electron content variations during an HSS/SIR-driven geomagnetic storm at high and mid latitudes. J Geophys Res (Space Phys) 129(12):033192. https://doi.org/10.1029/2024JA033192

Gillies RG, Hussey GC, Sofko GJ, McWilliams KA, Fiori RAD, Ponomarenko P, St.-Maurice, J.-P. (2009) Improvement of superdarn velocity measurements by estimating the index of refraction in the scattering region using interferometry. J Geophys Res Space Phys 114:234. https://doi.org/10.1029/2008JA013967

Gillies DM, Donovan E, Hampton D, Liang J, Connors M, Nishimura Y, Gallardo-Lacourt B, Spanswick E (2019) First observations from the TREx spectrograph: the optical spectrum of STEVE and the picket fence phenomena. Geophys Res Lett 46(13):7207–7213. https://doi.org/10.1029/2019GL083272

Gillies DM, Liang J, Gallardo-Lacourt B, Donovan E (2023) New insight into the transition from a SAR Arc to STEVE. Geophys Res Lett 50(6):101205. https://doi.org/10.1029/2022GL101205

Gololobov A, Shiokawa K, Baishev D, Inaba Y, Otsuka Y, Connors M (2023) Multi-event conjugate measurements of the sar arc detachment from the auroral oval using dmsp satellites and an all-sky camera at athabasca, canada. J Geophys Res Space Phys 128(4):030544. https://doi.org/10.1029/2022JA030544

Goodwin LV, St-Maurice J-P, Akbari H, Spiteri RJ (2018) Incoherent scatter spectra based on monte carlo simulations of ion velocity distributions under strong ion frictional heating. Radio Sci 53(3):269–287. https://doi.org/10.1002/2017RS006468

Grandin M, Aikio AT, Kozlovsky A, Ulich T, Raita T (2015) Effects of solar wind high-speed streams on the high-latitude ionosphere: superposed epoch study. J Geophys Res Space Phys 120(12):10669–10687. https://doi.org/10.1002/2015JA021785

Grandin M, Palmroth M, Whipps G, Kalliokoski M, Ferrier M, Paxton LJ, Mlynczak MG, Hilska J, Holmseth K, Vinorum K, Whenman B (2021) Large-scale dune aurora event investigation combining citizen scientists' photographs and spacecraft observations. AGU Adv 2(2):000338. https://doi.org/10.1029/2020AV000338

Grandin M, Bruus E, Ledvina VE, Partamies N, Barthelemy M, Martinis C, Dayton-Oxland R, Gallardo-Lacourt B, Nishimura Y, Herlingshaw K, Thomas N, Karvinen E, Lach D, Spijkers M, Bergstrand C (2024) The Gannon Storm: citizen science observations during the geomagnetic superstorm of 10 May 2024. Geosci Commun 7(4):297–316. https://doi.org/10.5194/gc-7-297-2024

Harding BJ, Mende SB, Triplett CC, Wu Y-JJ (2020) A mechanism for the STEVE continuum emission. Geophys Res Lett 47(7):087102. https://doi.org/10.1029/2020GL087102

Harel M, Wolf RA, Reiff PH, Spiro RW, Burke WJ, Rich FJ, Smiddy M (1981) Quantitative simulation of a magnetospheric substorm 1. Model logic and overview. J Geophys Res Space Phys 86(A4):2217–2241. https://doi.org/10.1029/JA086iA04p02217

He F, Zhang X-X, Chen B (2014) Solar cycle, seasonal, and diurnal variations of subauroral ion drifts: Statistical results. J Geophys Res Space Phys 119(6):5076–5086. https://doi.org/10.1002/2014JA019807

He F, Yao Z, Ni B, Cao X, Ye S, Guo R, Li J, Ren Z, Yue X, Zhang Y, Wei Y, Zhang X, Pu Z (2023) Sawtooth and dune auroras simultaneously driven by waves around the plasmapause. Earth Planet Phys 7(2):237–246. https://doi.org/10.26464/epp2023023

Heppner JP, Maynard NC (1987) Empirical high-latitude electric field models. J Geophys Res Space Phys 92(A5):4467–4489. https://doi.org/10.1029/JA092iA05p04467

Herlingshaw K, Lach D, Dayton-Oxland R, Bruus E, Karvinen E, Ledvina V, Partamies N, Grandin M, Spijkers M, Nishimura Y, Knudsen D, Ladbrook L, Martinis C, Gallardo-Lacourt B, Dyer A, Mielke L, Ratzlaff C, Evans L, Helin M, Kuzub J, Mathieu B, Thomas N, Glad M, Donovan E, Syrjäsuo M, Cordon S, Andersen J, Legg C (2024) ARCTICS aurora field guide and handbook for citizen science. Zenodo. https://doi.org/10.5281/zenodo.13932081

Hong J, Kim J-H, Chung J-K, Kim YH, Kam H, Park J, Mendillo M (2020) Simultaneous observations of sar arc and its ionospheric response at subauroral conjugate points ($l \simeq 2.5$) during the st. patrick's day storm in 2015. J Geophys Res Space Phys 125(4):2019–027321. https://doi.org/10.1029/2019JA027321

Huba J, Krall J (2013) Modeling the plasmasphere with SAMI3. Geophys Res Lett 40(1):6–10. https://doi.org/10.1029/2012GL054300

Huba JD, Lu G (2024) Modeling equatorial plasma bubbles with SAMI3/WACCM-X: September 2017 storm. Geophys Res Lett 51(11):109071. https://doi.org/10.1029/2024GL109071

Huba JD, Maute A, Crowley G (2017) SAMI3_ICON: model of the ionosphere/plasmasphere system. Space Sci Rev 212(1–2):731–742. https://doi.org/10.1007/s11214-017-0415-z

Inaba Y, Shiokawa K, Oyama S-I, Otsuka Y, Oksanen A, Shinbori A, Gololobov AY, Miyoshi Y, Kazama Y, Wang S-Y, Tam SWY, Chang T-F, Wang B-J, Yokota S, Kasahara S, Keika K, Hori T, Matsuoka A, Kasahara Y, Kumamoto A, Kasaba Y, Tsuchiya F, Shoji M, Shinohara I, Stolle C (2020) Plasma and field observations in the magnetospheric source region of a stable auroral red (sar) arc by the arase satellite on 28 March 2017. J Geophys Res Space Phys 125(10):028068. https://doi.org/10.1029/2020JA028068

Inaba Y, Shiokawa K, Oyama S-I, Otsuka Y, Connors M, Schofield I, Miyoshi Y, Imajo S, Shinbori A, Gololobov AY, Kazama Y, Wang S-Y, Tam SWY, Chang T-F, Wang B-J, Asamura K, Yokota S, Kasahara S, Keika K, Hori T, Matsuoka A, Kasahara Y, Kumamoto A, Matsuda S, Kasaba Y, Tsuchiya F, Shoji M, Kitahara M, Nakamura S, Shinohara I, Spence HE, Reeves GD, Macdowall RJ, Smith CW, Wygant JR, Bonnell JW (2021) Multi-event analysis of plasma and field variations in source of stable auroral red (sar) arcs in inner magnetosphere during non-storm-time substorms. J Geophys Res Space Phys 126(4):029081. https://doi.org/10.1029/2020JA029081

Ishimoto M, Romick GJ, Meng C-I (1994) Model calculation of atmospheric emission caused by energetic O+ precipitation. J Geophys Res Space Phys 99(A1):435–447. https://doi.org/10.1029/93JA01148

Izvekova YN, Popel SI, Morozova TI, Kopnin SI (2025) Possible manifestation of dusty ionospheric plasmas during high-speed meteor showers. Icarus 429:116383. https://doi.org/10.1016/j.icarus.2024.116383

Jordanova VK, Torbert RB, Thorne RM, Collin HL, Roeder JL, Foster JC (1999) Ring current activity during the early B< 0 phase of the January 1997 magnetic cloud. J Geophys Res Space Phys 104(A11):24895–24914. https://doi.org/10.1029/1999JA900339

Knudsen DJ, Burchill JK, Buchert SC, Eriksson AI, Gill R, Wahlund J-E, Åhlen L, Smith M, Moffat B (2017) Thermal ion imagers and Langmuir probes in the Swarm electric field instruments. J Geophys Res Space Phys 122(2):2655–2673. https://doi.org/10.1002/2016JA022571

Kozyra JU, Nagy AF, Slater DW (1997) High-altitude energy source(s) for stable auroral red arcs. Rev Geophys 35(2):155–190. https://doi.org/10.1029/96RG03194

Kunduri BSR, Baker JBH, Ruohoniemi JM, Clausen LBN, Grocott A, Thomas EG, Freeman MP, Talaat ER (2012) An examination of inter-hemispheric conjugacy in a subauroral polarization stream. J Geophys Res Space Phys. https://doi.org/10.1029/2012JA017784

Kunduri BSR, Baker JBH, Ruohoniemi JM, Thomas EG, Shepherd SG, Sterne KT (2017) Statistical characterization of the large-scale structure of the subauroral polarization stream. J Geophys Res Space Phys 122(6):6035–6048. https://doi.org/10.1002/2017JA024131

Laakso H, Pfaff R (2023) Fast plasma drifts in the high latitude ionosphere. Geophys Res Lett 50(14):103566. https://doi.org/10.1029/2023GL103566

Landry RG, Anderson PC (2018) An auroral boundary-oriented model of subauroral polarization streams (SAPS). J Geophys Res Space Phys 123(4):3154–3169. https://doi.org/10.1002/2017JA024921

Lanzerotti LJ, Hasegawa A, Maclennan CG (1978) Hydromagnetic waves as a cause of a SAR arc event. Planet Space Sci 26(8):777–783. https://doi.org/10.1016/0032-0633(78)90008-9

Liang J, Donovan E (2024) Quantum calculation of the vibrational excitation of nitrogen molecules by fast ions: can it contribute to STEVE formation? Geophys Res Lett 51(17):110986. https://doi.org/10.1029/2024GL110986

Liang J, Donovan E, Jackel B, Spanswick E, Gillies M (2016) On the 630 nm red-line pulsating aurora: Red-line emission geospace observatory observations and model simulations. J Geophys Res Space Phys 121(8):7988–8012. https://doi.org/10.1002/2016JA022901

Liang J, Donovan E, Connors M, Gillies D, St-Maurice JP, Jackel B, Gallardo-Lacourt B, Spanswick E, Chu X (2019) Optical spectra and emission altitudes of double-layer STEVE: a case study. Geophys Res Lett 46(23):13630–13639. https://doi.org/10.1029/2019GL085639

Liang J, St-Maurice JP, Donovan E (2021) A time-dependent two-dimensional model simulation of lower ionospheric variations under intense SAID. J Geophys Res Space Phys 126(12):029756. https://doi.org/10.1029/2021JA029756

Liang J, St-Maurice J-P, Donovan EF (2022) Model simulation of SAID intensification in the ionosphere under a current generator: the role of ion pedersen transport. J Geophys Res Space Phys 127(11):030960. https://doi.org/10.1029/2022JA030960

Liang J, Gillies DM, Spanswick E, Donovan EF (2024) Converting TREx-RGB green-channel data to 557.7 nm auroral intensity: methodology and initial results. Earth Planet Phys 8(1):258–274. https://doi.org/10.26464/epp2023063

Lilensten J, Blelly PL (2002) The TEC and F2 parameters as tracers of the ionosphere and thermosphere. J Atmos Solar Terr Phys 64(7):775–793. https://doi.org/10.1016/S1364-6826(02)00079-2

Lin D, Sorathia K, Wang W, Merkin V, Bao S, Pham K, Wiltberger M, Shi X, Toffoletto F, Michael A, Lyon J, Garretson J, Anderson B (2021) The role of diffuse electron precipitation in the formation of subauroral polarization streams. J Geophys Res Space Phys 126(12):029792. https://doi.org/10.1029/2021JA029792

Lin D, Wang W, Garcia-Sage K, Yue J, Merkin V, McInerney JM, Pham K, Sorathia K (2022) Thermospheric neutral density variation during the "spacex'' storm: implications from physics-based whole geospace modeling. Space Weather 20(12):003254. https://doi.org/10.1029/2022SW003254

Lin D, Wang W, Merkin VG, Huang C, Oppenheim M, Sorathia K, Pham K, Michael A, Bao S, Wu Q, Zhang Y, Wiltberger M, Toffoletto F, Lyon J, Garretson J (2022) Origin of dawnside subauroral polarization streams during major geomagnetic storms. AGU Adv 3(4):000708. https://doi.org/10.1029/2022AV000708

Lin D, Wang W, Fok M-C, Pham K, Yue J, Wu H (2024) Subauroral red arcs generated by inner magnetospheric heat flux and by subauroral polarization streams. Geophys Res Lett 51(17):109617. https://doi.org/10.1029/2024GL109617

Liu H-L, Foster BT, Hagan ME, McInerney JM, Maute A, Qian L, Richmond AD, Roble RG, Solomon SC, Garcia RR, Kinnison D, Marsh DR, Smith AK, Richter J, Sassi F, Oberheide J (2010) Thermosphere extension of the whole atmosphere community climate model. J Geophys Res Space Phys 115:12. https://doi.org/10.1029/2010JA015586

Liu H-L, Bardeen CG, Foster BT, Lauritzen P, Liu J, Lu G, Marsh DR, Maute A, McInerney JM, Pedatella NM, Qian L, Richmond AD, Roble RG, Solomon SC, Vitt FM, Wang W (2018) Development and validation of the whole atmosphere community climate model with thermosphere and ionosphere extension (WACCM-X 2.0). J Adv Model Earth Syst 10(2):381–402. https://doi.org/10.1002/2017MS001232

Lobzin VV, Pavlov AV (1999) Correlations between SAR arc intensity and solar and geomagnetic activity. Ann Geophys 17:770–781. https://doi.org/10.1007/s00585-999-0770-5

Lomidze L, Burchill JK, Knudsen DJ, Kouznetsov A, Weimer DR (2019) Validity study of the swarm horizontal cross-track ion drift velocities in the high-latitude ionosphere. Earth Space Sci 6(3):411–432. https://doi.org/10.1029/2018EA000546

Lummerzheim D, Lilensten J (1994) Electron transport and energy degradation in the ionosphere: evaluation of the numerical solution, comparison with laboratory experiments and auroral observations. Ann Geophys 12(10–11):1039–1051. https://doi.org/10.1007/s00585-994-1039-7

Lummerzheim D, Galand M, Semeter J, Mendillo MJ, Rees MH, Rich FJ (2001) Emission of oi(630 nm) in proton aurora. J Geophys Res Space Phys 106(A1):141–148. https://doi.org/10.1029/2000JA002005

Lynch KA, McManus E, Gutow J, Burleigh M, Zettergren M (2022) An ionospheric conductance gradient driver for subauroral picket fence visible signatures near STEVE events. J Geophys Res Space Phys 127(12):030863. https://doi.org/10.1029/2022JA030863

MacDonald EA, Donovan E, Nishimura Y, Case NA, Gillies DM, Gallardo-Lacourt B, Archer WE, Spanswick EL, Bourassa N, Connors M, Heavner M, Jackel B, Kosar B, Knudsen DJ, Ratzlaff C, Schofield I (2018) New science in plain sight: citizen scientists lead to the discovery of optical structure in the upper atmosphere. Sci Adv 4(3):0030. https://doi.org/10.1126/sciadv.aaq0030

Macho EP, Bristow W, Gallardo-Lacourt B, Shepherd SG, Ruohoniemi JM, Correia E (2024) Exploring the relationship between STEVE and SAID during three events observed by SuperDARN. Front Astron Space Sci. https://doi.org/10.3389/fspas.2024.1422164

Makarevich RA, Kellerman AC, Devlin JC, Ye H, Lyons LR, Nishimura Y (2011) SAPS intensification during substorm recovery: a multi-instrument case study. J Geophys Res Space Phys 116(A11):11311. https://doi.org/10.1029/2011JA016916

Marchaudon A, Blelly P-L (2015) A new interhemispheric 16-moment model of the plasmasphere-ionosphere system: IPIM. J Geophys Res Space Phys 120(7):5728–5745. https://doi.org/10.1002/2015JA021193

Marchaudon A, Blelly P-L (2020) Impact of the dipole tilt angle on the ionospheric plasma as modeled with IPIM. J Geophys Res Space Phys 125(6):027672. https://doi.org/10.1029/2019JA027672

Marchaudon A, Blelly P-L, Grandin M, Aikio A, Kozlovsky A, Virtanen I (2018) IPIM modeling of the ionospheric F2 layer depletion at high latitudes during a high-speed stream event. J Geophys Res Space Phys 123(8):7051–7066. https://doi.org/10.1029/2018JA025744

Martinis C, Baumgardner J, Mendillo M, Taylor MJ, Moffat-Griffin T, Wroten J, Sullivan C, Macinnis R, Alford B, Nishimura Y (2019) First ground-based conjugate observations of stable auroral red (SAR) Arcs. J Geophys Res Space Phys 124(6):4658–4671. https://doi.org/10.1029/2018JA026017

Martinis C, Nishimura Y, Wroten J, Bhatt A, Dyer A, Baumgardner J, Gallardo-Lacourt B (2021) First simultaneous observation of steve and sar arc combining data from citizen scientists, 630.0 nm all-sky images, and satellites. Geophys Res Lett 48(8):092169. https://doi.org/10.1029/2020GL092169

Martinis C, Griffin I, Gallardo-Lacourt B, Wroten J, Nishimura Y, Baumgardner J, Knudsen DJ (2022) Rainbow of the night: first direct observation of a SAR Arc evolving into STEVE. Geophys Res Lett 49(11):098511. https://doi.org/10.1029/2022GL098511

Matsuo T (2020) Recent progress on inverse and data assimilation procedure for high-latitude ionospheric electrodynamics. In: Dunlop MW, Lühr H (eds) Ionospheric multi-spacecraft analysis tools: approaches for deriving ionospheric parameters. ISSI Scientific Report Series. Springer, Cham, pp 219–232. https://doi.org/10.1007/978-3-030-26732-2_10

Mende SB, Harris SE, Frey HU, Angelopoulos V, Russell C, Donovan E, Jackel B, Greffen M, Peticolas LM (2008) The THEMIS array of ground-based observatories for the study of auroral substorms. Space Sci Rev 141:357–387. https://doi.org/10.1007/s11214-008-9380-x

Mende SB, Harding BJ, Turner C (2019) Subauroral green STEVE Arcs: evidence for low-energy excitation. Geophys Res Lett 46(24):14256–14262. https://doi.org/10.1029/2019GL086145

Mendillo M, Baumgardner J, Wroten J, Martinis C, Smith S, Merenda K-D, Fritz T, Hairston M, Heelis R, Barbieri C (2013) Imaging magnetospheric boundaries at ionospheric heights. J Geophys Res Space Phys 118(11):7294–7305. https://doi.org/10.1002/2013JA019267

Mendillo M, Finan R, Baumgardner J, Wroten J, Martinis C, Casillas M (2016) A stable auroral red (SAR) arc with multiple emission features. J Geophys Res Space Phys 121(10):10564–10577. https://doi.org/10.1002/2016JA023258

Millward GH, Müller-Wodarg ICF, Aylward AD, Fuller-Rowell TJ, Richmond AD, Moffett RJ (2001) An investigation into the influence of tidal forcing on f region equatorial vertical ion drift using a global ionosphere-thermosphere model with coupled electrodynamics. J Geophys Res Space Phys 106(A11):24733–24744. https://doi.org/10.1029/2000JA000342

Mishin EV (2013) Interaction of substorm injections with the subauroral geospace: 1. Multispacecraft observations of SAID. J Geophys Res Space Phys 118(9):5782–5796. https://doi.org/10.1002/jgra.50548

Mishin EV (2023) The evolving paradigm of the subauroral geospace. Front Astron Space Sci. https://doi.org/10.3389/fspas.2023.1118758

Mishin E, Streltsov A (2021) 8. Mesoscale and small-scale structure of the subauroral geospace. American Geophysical Union (AGU), pp 139–158. https://doi.org/10.1002/9781119815617.ch8

Mishin E, Nishimura Y, Foster J (2017) SAPS/SAID revisited: a causal relation to the substorm current wedge. J Geophys Res Space Phys 122(8):8516–8535. https://doi.org/10.1002/2017JA024263

Moshupi MC, Anger CD, Murphree JS, Wallis DD, Whitteker JH, Brace LH (1979) Characteristics of trough region auroral patches and detached arcs observed by isis 2. J Geophys Res Space Phys 84(A4):1333–1346. https://doi.org/10.1029/JA084iA04p01333

Nakamizo A, Hiraki Y, Ebihara Y, Kikuchi T, Seki K, Hori T, Ieda A, Miyoshi Y, Tsuji Y, Nishimura Y, Shinbori A (2012) Effect of r2-fac development on the ionospheric electric field pattern deduced by a global ionospheric potential solver. J Geophys Res Space Phys 117(A9):09231. https://doi.org/10.1029/2012JA017669

Nishimura Y, Gallardo-Lacourt B, Zou Y, Mishin E, Knudsen DJ, Donovan EF, Angelopoulos V, Raybell R (2019) Magnetospheric signatures of STEVE: implications for the magnetospheric energy source and interhemispheric conjugacy. Geophys Res Lett 46(11):5637–5644. https://doi.org/10.1029/2019GL082460

Nishimura Y, Bruus E, Karvinen E, Martinis CR, Dyer A, Kangas L, Rikala HK, Donovan EF, Nishitani N, Ruohoniemi JM (2022) Interaction between proton aurora and stable auroral red Arcs unveiled by citizen scientist photographs. J Geophys Res (Space Phys) 127(7):30570. https://doi.org/10.1029/2022JA030570

Nishimura Y, Dyer A, Kangas L, Donovan E, Angelopoulos V (2023) Unsolved problems in strong thermal emission velocity enhancement (steve) and the picket fence. Front Astron Space Sci. https://doi.org/10.3389/fspas.2023.1087974

Nishimura Y, Gallardo-Lacourt B, Donovan EF, Angelopoulos V, Nishitani N (2024) Auroral and magnetotail dynamics during quiet-time steve and said. J Geophys Res Space Phys 129(11):032941. https://doi.org/10.1029/2024JA032941

Nishimura Y, Lyons LR, Deng Y, Sheng C, Bristow WA, Donovan EF, Angelopoulos V, Nishitani N (2024) Obtaining continental-scale, high-resolution 2-D ionospheric flows and application to meso-scale flow science. J Geophys Res (Space Phys) 129(8):032924. https://doi.org/10.1029/2024JA032924

Nishitani N, Ruohoniemi JM, Lester M, Baker JBH, Koustov AV, Shepherd SG, Chisham G, Hori T, Thomas EG, Makarevich RA, Marchaudon A, Ponomarenko P, Wild JA, Milan SE, Bristow WA, Devlin J, Miller E, Greenwald RA, Ogawa T, Kikuchi T (2019) Review of the accomplishments of mid-latitude super dual auroral radar network (SuperDARN) HF radars. Prog Earth Planet Sci. https://doi.org/10.1186/s40645-019-0270-5

Nygrén T, Aikio AT, Kuula R, Voiculescu M (2011) Electric fields and neutral winds from monostatic incoherent scatter measurements by means of stochastic inversion. J Geophys Res Space Phys. https://doi.org/10.1029/2010JA016347

Oksavik K, Greenwald RA, Ruohoniemi JM, Hairston MR, Paxton LJ, Baker JBH, Gjerloev JW, Barnes RJ (2006) First observations of the temporal/spatial variation of the sub-auroral polarization stream from the superdarn wallops hf radar. Geophys Res Lett. https://doi.org/10.1029/2006GL026256

Palmroth M, Grandin M, Helin M, Koski P, Oksanen A, Glad MA, Valonen R, Saari K, Bruus E, Norberg J, Viljanen A, Kauristie K, Verronen PT (2020) Citizen scientists discover a new auroral form: dunes provide insight into the upper atmosphere. AGU Adv 1(1):000133. https://doi.org/10.1029/2019AV000133

Palmroth M, Grandin M, Sarris T, Doornbos E, Tourgaidis S, Aikio A, Buchert S, Clilverd MA, Dandouras I, Heelis R, Hoffmann A, Ivchenko N, Kervalishvili G, Knudsen DJ, Kotova A, Liu H-L, Malaspina DM, March G, Marchaudon A, Marghitu O, Matsuo T, Miloch WJ, Moretto-Jørgensen T, Mpaloukidis D, Olsen N, Papadakis K, Pfaff R, Pirnaris P, Siemes C, Stolle C, Suni J, van den IJssel J, Verronen PT, Visser P, Yamauchi M (2021) Lower-thermosphere-ionosphere (LTI), (2021) Quantities: current status of measuring techniques and models. Ann Geophys 39(1):189–237. https://doi.org/10.5194/angeo-39-189-2021

Partamies N, Dayton-Oxland R, Herlingshaw K, Virtanen I, Gallardo-Lacourt B, Syrjäsuo M, Sigernes F, Nishiyama T, Nishimura T, Barthelemy M, Aruliah A, Whiter D, Mielke L, Grandin M, Karvinen E, Spijkers M, Ledvina V (2024) First observations of continuum emission in dayside aurora. EGUsphere 2024:1–28. https://doi.org/10.5194/egusphere-2024-3669

Pham KH, Zhang B, Sorathia K, Dang T, Wang W, Merkin V, Liu H, Lin D, Wiltberger M, Lei J, Bao S, Garretson J, Toffoletto F, Michael A, Lyon J (2022) Thermospheric density perturbations produced by traveling atmospheric disturbances during august 2005 storm. J Geophys Res Space Phys 127(2):030071. https://doi.org/10.1029/2021JA030071

Picone JM, Hedin AE, Drob DP, Aikin AC (2002) NRLMSISE-00 empirical model of the atmosphere: statistical comparisons and scientific issues. J Geophys Res Space Phys 107(A12):15–11516. https://doi.org/10.1029/2002JA009430

Puhl-Quinn PA, Matsui H, Mishin E, Mouikis C, Kistler L, Khotyaintsev Y, Décréau PME, Lucek E (2007) Cluster and DMSP observations of SAID electric fields. J Geophys Res Space Phys. https://doi.org/10.1029/2006JA012065

Qian L, Burns AG, Emery BA, Foster B, Lu G, Maute A, Richmond AD, Roble RG, Solomon SC, Wang W (2014) 7. The NCAR TIE-GCM. American Geophysical Union (AGU), pp 73–83. https://doi.org/10.1002/9781118704417.ch7

Rees MH, Roble RG (1975) Observations and theory of the formation of stable auroral red arcs. Rev Geophys 13(1):201–242. https://doi.org/10.1029/RG013i001p00201

Ribeiro AJ, Ruohoniemi JM, Ponomarenko PV, Clausen NLBH, Baker JB, Greenwald RA, Oksavik K, Larquier S (2013) A comparison of superdarn acf fitting methods. Radio Sci 48(3):274–282. https://doi.org/10.1002/rds.20031

Richmond AD (1992) Assimilative mapping of ionospheric electrodynamics. Adv Space Res 12(6):59–68. https://doi.org/10.1016/0273-1177(92)90040-5

Richmond AD, Ridley EC, Roble RG (1992) A thermosphere/ionosphere general circulation model with coupled electrodynamics. Geophys Res Lett 19(6):601–604. https://doi.org/10.1029/92GL00401

Richmond AD, Lu G, Emery BA, Knipp DJ (1998) The amie procedure: prospects for space weather specification and prediction. Adv Space Res 22(1):103–112. https://doi.org/10.1016/S0273-1177(97)01108-3

Robert E, Barthelemy M, Cessateur G, Woelfflé A, Lamy H, Bouriat S, Gullikstad Johnsen M, Brändström U, Biree L (2023) Reconstruction of electron precipitation spectra at the top of the upper atmosphere using 427.8 nm auroral images. J Space Weather Space Clim 13:30. https://doi.org/10.1051/swsc/2023028

Robinson R (2004) New techniques and results from incoherent scatter radars. URSI Radio Sci Bull 2004(311):79–94

Ruohoniemi JM, Baker KB (1998) Large-scale imaging of high-latitude convection with super dual auroral radar network hf radar observations. J Geophys Res Space Phys 103(A9):20797–20811. https://doi.org/10.1029/98JA01288

Salvat F, Barjuan L, Andreo P (2022) Inelastic collisions of fast charged particles with atoms: Bethe asymptotic formulas and shell corrections. Phys Rev A 105:042813. https://doi.org/10.1103/PhysRevA.105.042813

Sarris TE, Talaat ER, Palmroth M, Dandouras I, Armandillo E, Kervalishvili G, Buchert S, Tourgaidis S, Malaspina DM, Jaynes AN, Paschalidis N, Sample J, Halekas J, Doornbos E, Lappas V, Moretto Jørgensen T, Stolle C, Clilverd M, Wu Q, Sandberg I, Pirnaris P, Aikio A (2020) Daedalus: a low-flying spacecraft for in situ exploration of the lower thermosphere-ionosphere. Geosci Instrument Methods Data Syst 9(1):153–191. https://doi.org/10.5194/gi-9-153-2020

Sazykin S, Fejer BG, Galperin YI, Zinin LV, Grigoriev SA, Mendillo M (2002) Polarization jet events and excitation of weak sar arcs. Geophys Res Lett 29(12):26–1264. https://doi.org/10.1029/2001GL014388

Semeter J, Hunnekuhl M, MacDonald E, Hirsch M, Zeller N, Chernenkoff A, Wang J (2020) The mysterious green streaks below STEVE. AGU Adv 1(4):00183. https://doi.org/10.1029/2020AV000018310.1002/essoar.10502878.2

Shiokawa K, Hosokawa K, Sakaguchi K, Ieda A, Otsuka Y, Ogawa T, Connors M (2009) The optical mesosphere thermosphere imagers (omtis) for network measurements of aurora and airglow. AIP Conf Proc 1144(1):212–215. https://doi.org/10.1063/1.3169292

Smalley RE, Wharton L, Levy DH (1975) The fluorescence excitation spectrum of rotationally cooled NO2. J Chem Phys 63(11):4977–4989. https://doi.org/10.1063/1.431244

Solomon SC (2017) Global modeling of thermospheric airglow in the far ultraviolet. J Geophys Res Space Phys 122(7):7834–7848. https://doi.org/10.1002/2017JA024314

Solomon SC, Hays PB, Abreu VJ (1988) The auroral 6300 Å emission: observations and modeling. J Geophys Res Space Phys 93(A9):9867–9882. https://doi.org/10.1029/JA093iA09p09867

Solomon SC, Burns AG, Emery BA, Mlynczak MG, Qian L, Wang W, Weimer DR, Wiltberger M (2012) Modeling studies of the impact of high-speed streams and co-rotating interaction regions on the thermosphere-ionosphere. J Geophys Res Space Phys. https://doi.org/10.1029/2011JA017417

Southwood DJ, Wolf RA (1978) An assessment of the role of precipitation in magnetospheric convection. J Geophys Res Space Phys 83(A11):5227–5232. https://doi.org/10.1029/JA083iA11p05227

Spanswick E, Liang J, Houghton J, Chaddock D, Donovan E, Gallardo-Lacourt B, Keenan C, Rosehart J, Nishimura Y, Hampton D, Gillies M (2024) Association of structured continuum emission with dynamic aurora. Nat Commun 15(1):10802. https://doi.org/10.1038/s41467-024-55081-5

St-Maurice J-P, Schunk RW (1979) Ion velocity distributions in the high-latitude ionosphere. Rev Geophys 17(1):99–134. https://doi.org/10.1029/RG017i001p00099

Svaldi V, Matsuo T, Kilcommons L, Gallardo-Lacourt B (2023) High-latitude ionospheric electrodynamics during STEVE and non-STEVE substorm events. J Geophys Res Space Phys 128(4):030277. https://doi.org/10.1029/2022JA030277

Takagi Y, Shiokawa K, Otsuka Y, Connors M, Schofield I (2018) Statistical analysis of sar arc detachment from the main oval based on 11-year, all-sky imaging observation at athabasca, canada. Geophys Res Lett 45(21):11539–11546. https://doi.org/10.1029/2018GL079615

Toffoletto F, Sazykin S, Spiro R, Wolf R (2003) Inner magnetospheric modeling with the rice convection model. Space Sci Rev 107(1):175–196. https://doi.org/10.1023/A:1025532008047

Wang W, Talaat ER, Burns AG, Emery B, Hsieh S-Y, Lei J, Xu J (2012) Thermosphere and ionosphere response to subauroral polarization streams (SAPS): model simulations. J Geophys Res (Space Phys) 117(A7):07301. https://doi.org/10.1029/2012JA017656

Wang B, Li P, Huang J, Zhang B (2019) Nonlinear Landau resonance between EMIC waves and cold electrons in the inner magnetosphere. Phys Plasmas 26(4):042903. https://doi.org/10.1063/1.5088374

Whiter DK, Sundberg H, Lanchester BS, Dreyer J, Partamies N, Ivchenko N, Di Fraia MZ, Oliver R, Serpell-Stevens A, Shaw-Diaz T, Braunersreuther T (2021) Fine-scale dynamics of fragmented aurora-like emissions. Ann Geophys 39(6):975–989. https://doi.org/10.5194/angeo-39-975-2021

Woo SB, Wong SF (1971) Interpretation of rate constants measured in drift tubes in terms of cross sections. J Chem Phys 55(7):3531–3541. https://doi.org/10.1063/1.1676609

Yadav S, Shiokawa K, Oyama S, Inaba Y, Takahashi N, Seki K, Keika K, Chang T-F, Tam SWY, Wang B-J, Kazama Y, Wang S-Y, Asamura K, Kasahara S, Yokota S, Hori T, Kasaba Y, Tsuchiya F, Kumamoto A, Shoji M, Kasahara Y, Matsuoka A, Matsuda S, Jun C-W, Imajo S, Miyoshi Y,

Shinohara I (2021) Study of an equatorward detachment of auroral arc from the oval using ground-space observations and the bats-r-us–cimi model. J Geophys Res Space Phys 126(12):029080. https://doi.org/10.1029/2020JA029080

Yamakawa T, Seki K, Amano T, Takahashi N, Miyoshi Y (2019) Excitation of storm time pc5 ulf waves by ring current ions based on the drift-kinetic simulation. Geophys Res Lett 46(4):1911–1918. https://doi.org/10.1029/2018GL081573

Yamakawa T, Seki K, Amano T, Miyoshi Y, Takahashi N, Nakamizo A, Yamamoto K (2023) Effects of cold plasma on the excitation of internally driven ULF waves by ring current ions based on the magnetosphere-ionosphere coupled model. J Geophys Res Space Phys 128(9):031638. https://doi.org/10.1029/2023JA031638

Yin Q, Pham KH, Chen J, Zhang B (2024) Validation of simulated statistical characteristics of magnetosphere-ionosphere coupling in global geospace simulations over an entire carrington rotation. Space Weather 22(6):003749. https://doi.org/10.1029/2023SW003749

Yue X, Ning B, Jin L, Ding F, Ke C, Wang J, Zhang N, Cai Y, Li M, Luo J, Chen W, Zhang Y, Zhao B, Zeng L, Wang Y (2024) The Sanya incoherent scatter radar tristatic system and initial experiments. Space Weather 22(9):2024–003963. https://doi.org/10.1029/2024SW003963

Zhang Y, Gallardo-Lacourt B, Paxton LJ, Erickson PJ, Hairston M, Coley WR (2024) Steve events with fuv emissions. J Geophys Res Space Phys 129(2):032017. https://doi.org/10.1029/2023JA032017

Zhang J, Lan A, Yan J, Deng X, Wang W, Li H, Sun L, Nan Y, Song X, Wang C (2024) Development of the Chinese dual auroral radar network and preliminary results. Space Weather 22(10):004131. https://doi.org/10.1029/2024SW004131

Zou Y, Lyons LR, Shi X, Liu J, Wu Q, Conde M, Shepherd SG, Mende S, Zhang Y, Coster A (2022) Effects of subauroral polarization streams on the upper thermospheric winds during non-storm time. J Geophys Res (Space Phys) 127(5):29988. https://doi.org/10.1029/2021JA029988

Authors and Affiliations

Bea Gallardo-Lacourt[1,2] · Maxime Grandin[3] · Aurélie Marchaudon[4] · Mathieu Barthelemy[5,6]

✉ Bea Gallardo-Lacourt
bea.gallardolacourt@nasa.gov

Maxime Grandin
maxime.grandin@fmi.fi

Aurélie Marchaudon
aurelie.marchaudon@irap.omp.eu

Mathieu Barthelemy
mathieu.barthelemy@univ-grenoble-alpes.fr

1 Heliophysics Science Division, NASA, Goddard Space Flight Center, 8800 Greenbelt Rd, Greenbelt, MD 20771, USA

2 Department of Physics, The Catholic University of America, 620 Michigan Ave., N.E., Washington, DC 20064, USA

3 Finnish Meteorological Institute, Erik Palménin aukio 1, 00560 Helsinki, Finland

4 Institut de Recherche en Astrophysique et Planétologie, CNRS, CNES, Université de Toulouse, 9, Avenue du Colonel Roche, Toulouse, France

5 CNRS, IPAG, Univ. Grenoble Alpes, 414, Avenue de la Piscine, 38000 Grenoble, France

6 CSUG, Univ. Grenoble Alpes, 120, Avenue de la Piscine, 38000 Grenoble, France